A&A, 711, A67 (2026)
https://doi.org/10.1051/0004-6361/202659745

Astronomy & Astrophysics

Stellar rotation and binaries in open clusters with Gaia Data Release 3

E. Pancino[1,⋆], E. Reggiani[1,2], S. Marinoni[3], P. M. Marrese[3], D. Alvarez Garay[1], A. Avdeeva[1], M. Echeveste[1], E. Leitinger[1,4], S. Nedhath[1,2], S. Rani[1], N. Sanna[1], S. Saracino[1], L. Steinbauer[1,2], A. Turchi[1], V. V. Jadhav[5], S. Kamann[6], and M. Rainer[7]

[1] INAF – Osservatorio Astrofisico di Arcetri, Largo E. Fermi 5, 50125 Firenze, Italy
[2] Dipartimento di Fisica e Astronomia, Università di Firenze, Via G. Sansone 1, 50019 Sesto Fiorentino, FI, Italy
[3] INAF – Osservatorio Astronomico di Roma, Via Frascati 33, 00040 Monte Porzio Catone, Roma, Italy
[4] Dipartimento di Fisica e Astronomia, Università degli Studi di Bologna, Via Gobetti 93/2, 40129 Bologna, Italy
[5] Astronomical Institute, Faculty of Mathematics and Physics, Charles University, V Holešovičkách 2, CZ-180 00 Praha 8, Czech Republic
[6] Astrophysics Research Institute, Liverpool John Moores University, IC2 Liverpool Science Park, 146 Brownlow Hill, Liverpool L3 5RF, United Kingdom
[7] INAF – Osservatorio Astrofisico di Torino, Strada Osservatorio 20, 10025 Pino Torinese, TO, Italy

Received 6 March 2026 / Accepted 30 April 2026

ABSTRACT

Context. Stellar rotation is a fundamental ingredient in shaping the evolution of stars, and it can also be used to trace past stellar interactions. Yet, systematic studies of stellar rotation in large samples of stars belonging to different populations have only recently been made possible, thanks to spectroscopic surveys.

Aims. We used the catalogue of rotational broadening and rotation periods released with *Gaia* Data Release 3 (DR3). We focused on open clusters to study the rotational behavior of several interesting populations including, among others, blue stragglers and extended main-sequence turnoffs (eMSTOs).

Methods. We used literature lists of almost a million member stars in several thousand open clusters in the Milky Way. We collect properties of stars and clusters from large surveys, including *Gaia*, and from various literature sources. We included a comprehensive collection of known variables and binary stars from various databases. We manually selected (exotic) stellar populations from the color–magnitude diagrams of individual clusters and studied their rotational properties.

Results. Our catalog contains more than 44 000 rotationally characterized stars, almost 57 000 variables (excluding binaries), and more than 22 000 binary stars. We find several interesting results, including a few hundred new blue stragglers and several fast-rotating red giants, and we increased the number of clusters with an eMSTO to 96. We discovered that most clusters more massive than 10^3 $M_\odot$ display an eMSTO. We present a new parametrization of the number of blue stragglers as a function of cluster mass and age. We find that the percentage of binary stars in the equal-mass binary sequence and in the main sequence are similar.

Conclusions. We present the first large-scale statistical exploration of stellar rotation in open clusters, which already yielded new interesting results and can be used as the basis for several detailed follow-up studies.

Key words. surveys – binaries: general – stars: rotation – stars: variables: general – open clusters and associations: general

1. Introduction

Stellar rotation rates are a necessary ingredient for understanding how stars form, their evolutionary pathways, and their surface chemistry, among others. Stellar rotation significantly affects internal processes, such as mixing and angular-momentum transport. For instance, fast-rotating stars may exhibit enhanced chemical mixing, influencing isotopic ratios such as [C/O] and [N/O], which provide insights into stellar evolution stages (Zahn 1992; Maeder & Meynet 2000). Fast-rotating massive stars were in fact key to explaining the primary nitrogen production observed in Milky Way stellar abundance ratios (Meynet & Maeder 2002). Stellar rotation is also important in the context of the evolution of binary star systems. Interaction in close binaries can result in tidal locking and synchronization, while mass-transfer episodes can also transfer considerable angular momentum (Hut 1981; Soberman et al. 1997; Hurley et al. 2002). Such interactions can lead to significant changes in the rotation rates and in the subsequent evolution of the stars involved. Stellar rotation rates can also influence the mass loss and wind properties in massive stars (Smith 2014). Finally, stellar rotation evolves naturally during the life of stars, particularly low-mass stars, because of magnetic braking, opening up the possibility of stellar dating techniques such as gyrochronology (Kraft 1967; Skumanich 1972; Soberman et al. 1997). Systematic measurements of stellar rotation rates across the whole parameter space of stellar properties and environments require exceptional observational efforts. In particular, photometric monitoring and asteroseismic surveys (see Appendix D.1 for references) have provided large samples of rotational-period measurements, while large spectroscopic surveys (see Sect. 2.3 for references) have provided spectral line-broadening measurements for even larger samples.

⋆ Corresponding author.

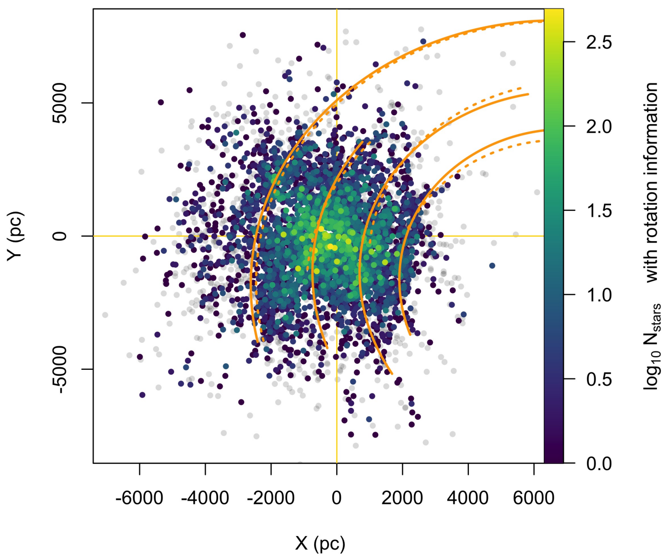

Fig. 1. Studied clusters in Galactic cartesian coordinates. All clusters are plotted in gray in the background. Clusters are colored based on the number of stars with rotation information. The color scale saturates at about 400 for clarity, but several clusters have up to a few thousand members with rotation information. The spiral arms of the Milky Way, as modeled by Castro-Ginard et al. (2021) and Reid et al. (2014), are plotted as solid and dashed orange lines, respectively.

Here, we focus on open clusters, which offer the unique opportunity to obtain accurate age and distance estimates for hundreds of thousands of member stars. More specifically, the *Gaia* mission (Gaia Collaboration 2016) has drastically improved our samples of open clusters and member stars, among many other results. In particular, the third *Gaia* data release (hereafter DR3, Gaia Collaboration 2023c), provides parameters related to the rotational characterization of stars for the first time (see Sect. 2.3 for more details and references). Although these measurements are expected to improve in future releases and are subject to some limitations, the sheer amount of characterized stars opens the possibility to carry out an exploratory study, a statistical overview of open cluster stars across the color–magnitude diagram (CMD), which can provide a useful starting point for more detailed investigations.

The paper is organized as follows: our sample is presented in Sect. 2; we explore the rotational properties of different stellar populations, including exotic ones, in Sect. 3; we summarize our main results and present our conclusions in Sect. 4. Further details on the characterization of member stars and clusters, as well as additional figures, are presented in the appendices.

2. Sample selection and characterization

2.1. Open-cluster list

Since the advent of the *Gaia* space mission (Gaia Collaboration 2016), the census of existing open clusters has undergone a revolution (see Fig. 1 and Table 1 by Perren et al. 2023), with significant increases in sample size and data quality compared to previous efforts (Kharchenko et al. 2013; Dias et al. 2002). In this panorama, the most comprehensive effort was conducted by Hunt & Reffert (2021, 2023, 2024), based on *Gaia* DR3 astrometry and photometry (Gaia Collaboration 2023c). We based our work mostly on their catalog, integrated with literature data as described in the appendices. There are 5647 open clusters (`kind = "o"`) listed by Hunt & Reffert (2024). However, the authors note that ≃10–20% of the well-known clusters in the literature were not found with their method. For this reason, we identified 51 missing clusters possessing good *Gaia* data, which were added to our cluster master list (see Appendix A for details).

Table 1. Catalogue of clusters for which at least one member star has a *Gaia* DR3 `vbroad`, `vsini`, or `prot` estimate, with selected properties.

Quantity	Units	Description
Cluster		Adopted cluster name
AltNames		Other cluster names
RA_0	deg	Central Right Ascension
Dec_0	deg	Central Declination
pmRA*	mas/yr	Mean proper motion in RA
pmDec	mas/yr	Mean proper motion in Dec
ϖ	mas	Mean parallax
X	pc	X in Galactic cartesian coordinates
Y	pc	Y in Galactic cartesian coordinates
Z	pc	Z in Galactic cartesian coordinates
Dist	pc	Distance from the cluster
R_{GC}	pc	Galactocentric distance
R_{50}	deg	Radius enclosing half members
R_J	deg	Jacobi radius
n_{mem}		Number of cluster members
sourceAstro		Literature source of astrometry
RV	km s^{-1}	Mean RV for the cluster
n_{RV}		Stars used for RV
SourceRV		Literature source for RV
[Fe/H]	dex	Mean iron metallicity of the cluster
$n_{[Fe/H]}$		Stars used for [Fe/H]
SourceFeH		Literature source of [Fe/H]
log(age)	yr	Logarithmic age of the cluster
SourceAge		Literature source of log(age)
A_V	mag	Absorption in the *V* band
mass	$M_\odot$	Cluster mass
has_rot		≥1 star with rotation information

Notes. See Section C.3 for more details. The table is available electronically at the CDS, where reported quantities are accompanied by their uncertainties.

Figure 1 shows the spatial distribution of our sample clusters. We also critically compiled cluster properties from the literature and redetermined some of them using information from *Gaia* DR3 and from spectroscopic surveys, as described in full detail in Appendix A. The final list of clusters with their selected properties can be found in Table 1, which is available electronically.

2.2. Member-star list

The list of member stars published by Hunt & Reffert (2024) contains more than 700 000 stars belonging to open clusters, out of a total of almost 1.3 million stars. After a series of extensive comparisons with other member lists in the literature, we found several advantages to using the Hunt & Reffert (2024) list: their work is based on *Gaia* DR3, while several other lists are based on DR2; the CMDs appear cleaner and better defined; stars belonging to the tidal tails of clusters are included; and the magnitude limit is deeper than several previous searches, reaching G ≃ 20 instead of 18 mag. To integrate the Hunt & Reffert (2024) member list with the 51 missing clusters mentioned in Sect. 2.1 and to characterize their properties, we relied on our own critically

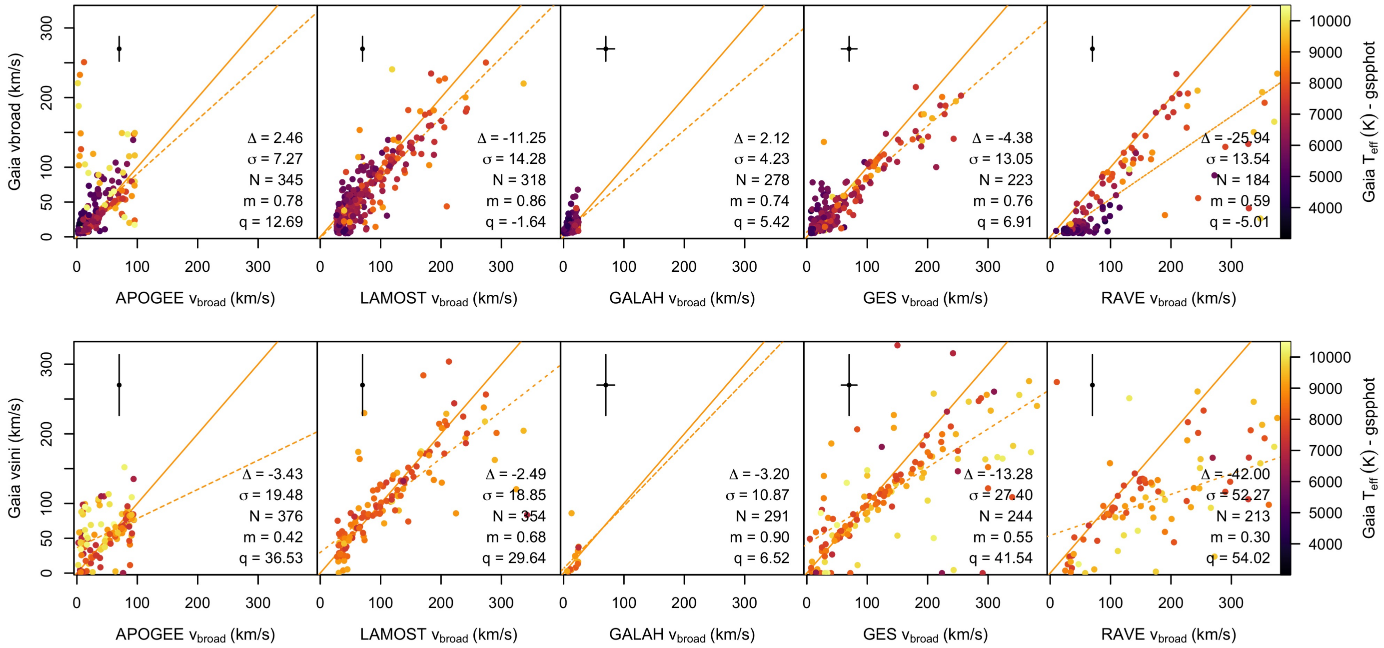

Fig. 2. Comparison of *Gaia* DR3 `vbroad` (top panels) and `vsini` (bottom panels) estimates with those of five spectroscopic surveys. The one-to-one agreement is reported in each panel as a solid orange line, while a linear fit to the data is reported as a dashed line. Annotated in each panel are the median difference (Δ), the median absolute deviation (MAD, σ), the number of stars (N), the angular coefficient (m), and the intercept (q) of the linear fit. Points are colored according to $T_{\rm eff}$.

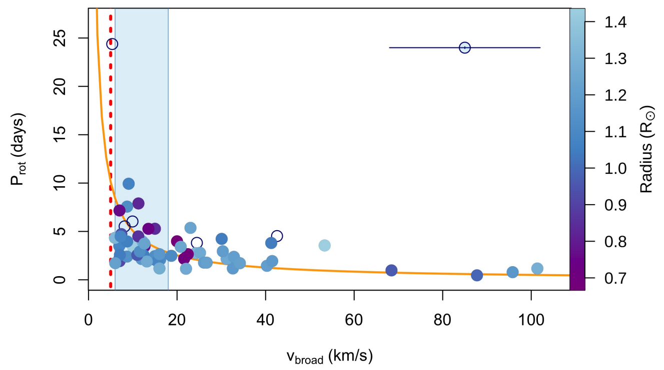

Fig. 3. Relation between `prot` and `vbroad/vsini` for the 65 dwarf stars that have both measurements. The region where `vbroad` starts to be overestimated is shaded in light blue, the filtering at 5 km s^{-1} is represented by a dashed red line, and the expected relationship for a 1 $R_\odot$ star with $\sin i = 1$ is plotted in orange. The typical (median) error bar of the 65 stars is plotted in the upper right corner. Stars are colored according to their radius (empty symbols indicate stars without a radius estimate).

compiled collection of literature sources, as discussed in details in Appendix C. We also performed a comprehensive literature search to identify known variable and binary stars, as described in detail in Appendix D.

2.3. Information on stellar rotation from Gaia DR3

The *Gaia* DR3 catalog provides three means of characterizing stellar rotation. The first is the rotational broadening measured on the Radial Velocity Spectrometer (RVS) spectra (Gaia Collaboration 2016; Cropper et al. 2018; Katz et al. 2023); we refer to this measurement as `vbroad`. More details about its strengths and limitations can be found in Appendix B.1 and in Frémat et al. (2023). We complemented the `vbroad` measurements with the `vsini_esphs` ones (hereafter `vsini`) obtained for hot stars from a combination of RVS spectra and spectrophotometry and described in more detail in Appendix B.2. These measurements are more scattered than the `vbroad` ones, so we mostly rely on `vbroad` in the following. Additionally, we used the rotational periods (`best_rotation_period`) obtained from the characterization of spotted rotating stars (hereafter `prot`), which are described in more detail in Appendix B.3 and in Lanzafame et al. (2018) and Distefano et al. (2023).

A comparison of `vbroad` and `vsini` with the values provided in the main spectroscopic surveys is presented in Fig. 2. In particular, we compare with the line broadening measured by APOGEE DR17 (Abdurro'uf et al. 2022), LAMOST DR10[1], GALAH DR4 (Buder et al. 2025), Gaia-ESO DR5.1 (Gilmore et al. 2012; Randich et al. 2022), and RAVE DR6 (Steinmetz et al. 2020). As can be seen, the overall agreement is satisfactory, considering the large uncertainties of this type of measurement and the validity limits of each survey. The comparison confirms the tendency of *Gaia* measurements to be underestimated for stars hotter than about 7500 K (see especially the two rightmost panels of Fig. 2). We also stress here that there appear to be residual biases of up to ≃50 km s^{-1} for stars hotter than ≃7000 K as the G magnitude becomes fainter (see Fig. 14 by Frémat et al. 2023). As an overall sanity check, we compared `prot` with `vbroad` (complemented by `vsini`) for the 65 stars in our sample that have both measurements. As can be seen from Fig. 3, the two estimates roughly follow the expected trend and are broadly consistent with each other, which is more than satisfactory, especially when considering the uncertainties of the `vbroad` and `vsini` determination process.

[1] http://lamost.org/dr10/

Table 2. Catalog of member stars in the full sample, along with some fundamental properties obtained from *Gaia* DR3 and other literature sources.

Column	Units	Description
source_id		*Gaia* DR3 identifier
Cluster		Adopted cluster name
RA	deg	Right Ascension
Dec	deg	Declination
μ^*_{RA}	mas yr^{-1}	RA proper motion
μ_{Dec}	mas yr^{-1}	Dec proper motion
ϖ	mas	Parallax
G	mag	*G*-band magnitude
G_{BP}	mag	BP magnitude
G_{RP}	mag	RP magnitude
$E(G_{BP}–G_{RP})$	mag	Reddening
A_G	mag	Absorption
RV	km s^{-1}	Radial velocity
RV_mem		Radial velocity membership (yes, no, maybe, or empty)
`vbroad`	km s^{-1}	Rotational broadening RVS
`vsini`	km s^{-1}	Rotational broadening ESP-HS
`prot`	days	Rotation period
A_{max}	mag	Photospheric activity
T_{eff}	K	Effective temperature
log*g*	dex	Surface gravity
[Fe/H]	dex	Iron metallicity
M	$M_\odot$	Mass
R	$R_\odot$	Radius
flag_var		variability flag (Table D.1) (`VAR`, `VAR:`, or empty)
flag_bin		binarity flag (Table D.2) (`BIN`, `BIN:`, or empty)
star_sample		See Sect. 3

Notes. See Appendix C for more details. Each property is accompanied by its uncertainty in the full electronic version of the table at the CDS.

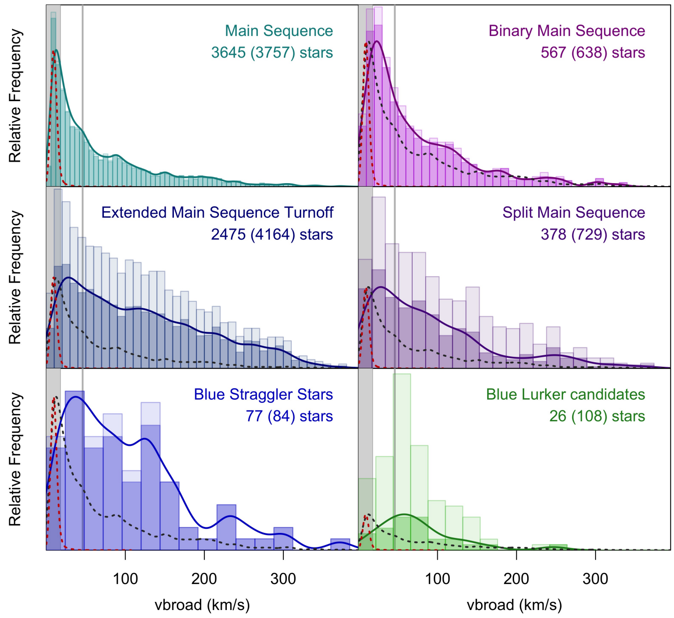

Fig. 4. Distribution of `vbroad` of dwarf samples analyzed in Sect. 3. In each panel, the generalized histograms of the MS and RGB samples are reported as a gray and a red dashed line, respectively. Lighter shaded histograms also include less certain sample members. Darker histograms show only the best members (sample sizes in parentheses). The gray shaded area (`vbroad` < 20 km s^{-1}) in each panel represents the region where `vbroad` starts to be overestimated. The vertical gray line at 46 km s^{-1} represents twice the RVS resolution. Given the diversity of sample sizes, the vertical axes have different (linear) scales.

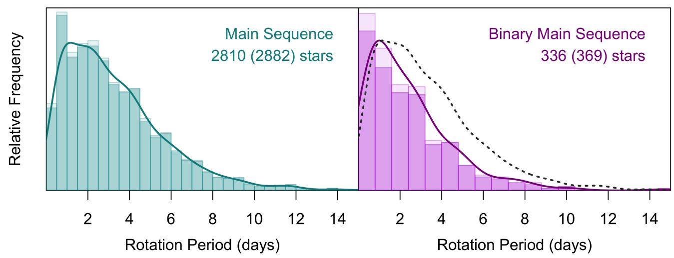

Fig. 5. Similar to Fig. 4, but for the rotation periods, which are only available for the MS and binMS samples.

3. Stellar rotation across the CMD

To study the rotational properties of our sample stars, we subdivided them in different samples, indicated in the `star_sample` field in Table 2. The selections were done semi-manually, using strictly the data distribution on the CMD of each individual cluster, as further described below. For this reason, we focused on clusters with relatively low reddening (and apparent differential reddening ≲0.5 mag) and with a sufficient number of stars (≳10) in the relevant sequences. We used solar-scaled, solar metallicity BaSTI[2] isochrones and the solar metallicity zero-age MS (ZAMS, Hidalgo et al. 2018), with the appropriate cluster parameters from Table 1, exclusively to guide the eye and to double-check the cluster parameters. Even if the literature parameters are mostly obtained with PARSEC isochrones, the two sets are comparable for the purpose of the present qualitative study (see Hidalgo et al. 2018; Nguyen et al. 2022; Boin et al. 2026, for comparisons). To provide an overview of the data in hand, we show in Appendix B a few CMDs and Kiel diagrams showing the position, properties, and fraction of stars with rotational properties. In the following sections we describe and discuss our results, separately for each of the selected samples.

3.1. Main and binary sequence

Main-sequence (MS) stars were selected as being within 3 MAD (median absolute deviation) from a smooth-spline fit to the MS ridge line. The binary MS sample (hereafter binMS) was selected in a similar way, by shifting the spline fit up by 0.75 mag[3]. In clusters with slightly higher differential reddening (but always ≲0.5 mag), we used the midpoint between the two fits to separate MS and binMS. Thus, our binMS sample is mostly composed of binaries with similar masses (q ≳ 0.5–0.6), but this varies depending on how tight the MS of each cluster is. Examples of sample selections are presented in Appendix E.1. We further excluded more than 100 abnormally fast rotators, which we flag as candidate blue lurkers (BL), as discussed in detail in Appendix E.2.

The `vbroad` distribution of the MS and binMS samples is shown in Fig. 4, while the `prot` distribution is shown in Fig. 5.

[2] http://basti-iac.oa-abruzzo.inaf.it/isocs.html

[3] This corresponds to twice the flux of an MS star.

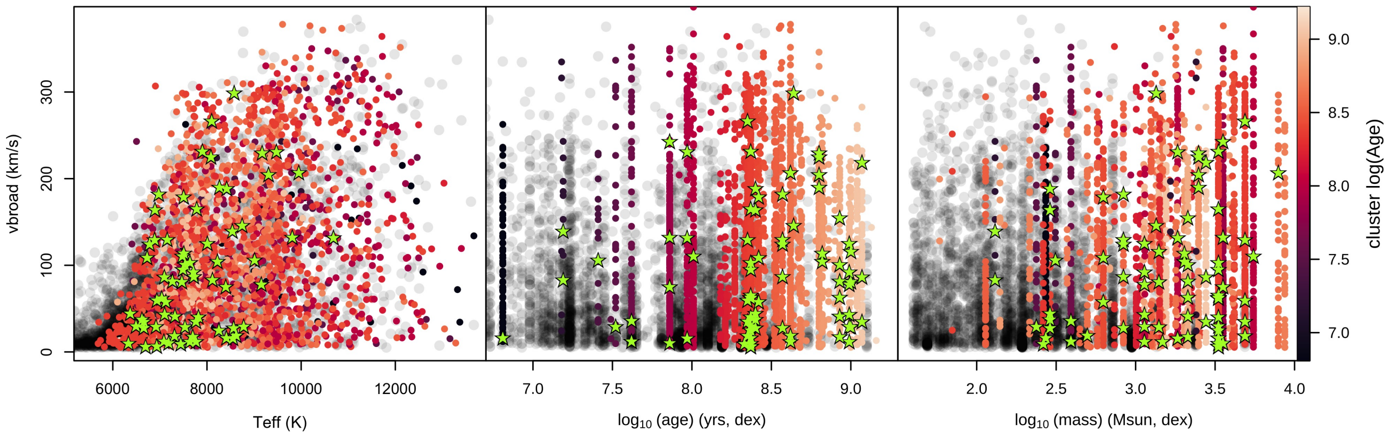

Fig. 6. Comparison of the spread in `vbroad` between normal MS stars in clusters showing no sign of an eMSTO (gray points) and stars in the eMSTO region in clusters with a confirmed eMSTO (points colored by age), as a function of T_{eff} of the stars (left panel), cluster age (middle panel), and cluster mass (right panel). Binary stars in the eMSTO sample are plotted as green stars.

The long tail of fast rotators in the MS `vbroad` sample is dominated by early type stars, where we excluded the stars belonging to extended MS turnoffs (eMSTOs, see Sect. 3.2), while the flat peak in the MS `prot` distribution is mostly caused by cool and low-mass fast rotators. The MS and binMS distributions have different `vbroad` peaks, at about 15 and 20 km s^{-1}, respectively. While the MS peak is in the `vbroad` saturation region, and thus compatible with no rotation, the binMS peak is slightly outside of it. We also observe a different shape in the MS and binMS `vbroad` samples, resembling a sort of systematic shift of $\lesssim$ 30–50 km s^{-1} towards higher `vbroad`. A two-sample KS test – that the distributions are extracted from the same parent distribution – returns P-values of 0.0001 and $1.09 \cdot 10^{-10}$ in the case of `vbroad` and `prot`, respectively. Unresolved spectroscopic SB2 binaries could mimic a higher rotation (Simonian et al. 2020), thus we draw a line in Fig. 4 at 46 km s^{-1}, which is twice the resolution of *Gaia* RVS. Stars with `vbroad` above the line definitely cannot be unresolved SB2. This is slightly pessimistic, given that in reality `vbroad` starts to saturate at 18–20 rather than 23 km s^{-1} (see Appendix B). Therefore, a more likely explanation is that in the binMS there are more interacting or post-interaction binaries, which have been spun-up.

We find comparable proportions of binaries in the MS and binMS samples, i.e., about 7 and 6%, respectively. We did not spot any obvious difference in the types of binaries found in the two samples. If we assume that the two samples suffer from similar selection biases, we find that the ratio between binaries with $q \gtrsim 0.6$ and those with $q \lesssim 0.6$ is about 0.8 (see Appendix E.1 for more details). A flat q distribution would have 0.7. Our data thus support q distributions that include a significant proportion of low mass ratios (see, e.g. Kähler 1999). In any case, because of the reasons described more in details in Appendix E.1, we refrain from computing cluster binary fractions using photometric criteria.

3.2. Extended MS turnoffs

Extended MS turnoffs (eMSTOs) were initially identified in clusters in the Magellanic Clouds as fan-shaped or bimodal turnoff regions (Bertelli et al. 2003; Mackey & Broby Nielsen 2007). After a long debate about whether the spread was caused by age differences or stellar rotation (Goudfrooij et al. 2014; Niederhofer et al. 2015), the general consensus finally settled on a spread in stellar rotation, supported by direct measurements in Milky Way open clusters (Bastian et al. 2018; Deng & Li 2024; Cordoni et al. 2024, and references therein). However, there are hints that stellar models including rotation do not always fully account for the observed photometric spreads (Georgy et al. 2013; Correnti et al. 2017; Kamann et al. 2023; Cordoni et al. 2024). Furthermore, there is no established explanation for why stars should display different rotation. A few possibilities have been put forth (e.g. D'Antona et al. 2017; Bastian et al. 2020; Wang et al. 2022), involving non-canonical stellar evolutionary paths, mediated by binary interactions or early stellar and disk evolution. Observationally, the eMSTO phenomenon was found in several clusters, mostly in the range from 100 Myrs to 2 Gyrs, with some exceptions.

We could identify 96 clusters with a clear eMSTO and 268 with some form of unusual TO regions (labelled as `eMSTO:` in Table 2), significantly increasing the number of known clusters with this feature in the literature, which was a few tens (Cordoni et al. 2024). We manually selected the eMSTO stars when the spread at the TO was visually larger than on the MS below. We also required that the spread was accompanied by some segregation in the `vbroad` and `vsini` on the blue and red sides of the TO region. However, we included about a dozen clusters without `vbroad` or `vsini` information, either because the photometric signature was sufficiently clear or the case was already known in the literature (one example is NGC 2818). A few clusters with a clear eMSTO are presented in Appendix E.3, sorted by decreasing age. We note that in several clusters there are a few fast-rotating stars (>150 km s^{-1}) on the blue side of the eMSTO (see e.g. NGC 5822 in Appendix E.3). If the eMSTO morphology was solely driven by stellar rotation, we would expect some low-`vbroad` stars on the red side (because of the sin*i* projection), but not high-`vbroad` stars on the blue side. These stars are still within the eMSTO region, so we find it unlikely that they are BSS or post-transfer binaries. If this is confirmed, we can consider these stars as additional evidence that a more complex explanation must be invoked, involving more profound structural changes in eMSTO stars (Johnston et al. 2019, see Fig. 3).

One unique advantage of our sample is that we can compare a large number of confirmed eMSTO stars with rotation information ($\simeq$6000) with the MS sample, selected to be in the same range of T_{eff} and $\log g$ ($\simeq$ 8000 stars with rotation information), as shown in Fig. 6. By comparing Figs. 4 and 6, we observe that the width in the vbroad distribution is roughly comparable between the two samples, but the shape of the distribution is different: normal MS stars are more peaked towards low vbroad than the eMSTO stars. A K-S test returns a p-value of $<2.2 \cdot 10^{-16}$. If we assume that the stellar rotation angles are randomly distributed, this suggests a larger proportion of fast rotators in eMSTO stars than in the MS of normal clusters, but we should keep in mind that the vbroad distribution within individual clusters can vary (see Santos et al. 2025).

By inspecting Fig. 6 we note a few more differences. As a function of $T_{\rm eff}$, the MS and eMSTO distributions are roughly similar, in the sense that the upper envelopes are compatible. This shows that, to first order, the maximum vbroad is driven by the rotational properties of stars of different masses. However, if we plot vbroad as a function of cluster age, we see that above ≃100 Myr, the eMSTO stars vbroad spread seems to globally decrease with increasing age. At older ages the stellar masses in the TO region are lower and we should expect generally lower vbroad values. This decreasing spread of vbroad at old ages seems to contradict the increase of the photometric spread, which is found both when measured as an apparent age spread (Niederhofer et al. 2015) or a pseudo-color spread (Cordoni et al. 2024). Detailed simulations would be useful to assess whether these two opposite trends are expected on the basis of gravity darkening or whether other structural changes in the star are required to reproduce the observations. Finally, when we plot vbroad as a function of cluster mass, we see that at masses above ≃1000 $M_{\odot}$ there is almost no cluster without an eMSTO (gray dots in Fig. 6), thus cluster mass seems to play an important role in the emergence of the eMSTO phenomenon and indeed eMSTOs were first discovered in massive clusters in the Magellanic Clouds. We also see very few clusters with an eMSTO below 1000 $M_{\odot}$, but this could in part be due to the fact that eMSTOs are more difficult to detect when there are few stars.

To test the idea that binary interactions may cause eMSTO (D'Antona et al. 2015), we study 208 binaries (green star symbols in Fig. 6) and 131 suspected binaries in the eMSTO sample. Most are eclipsing and SB1, with a couple of G Cas variables, and a triple system in NGC 2516 (Mermilliod et al. 2008, 2009). We note that they are mostly cooler than 10 000 K and mostly found in more massive clusters. The median vbroad of the binaries in the eMSTO sample is comparable to that of the whole sample: 90 versus 110 km s^{-1}. We do not observe any obvious preference for the binaries to lie on the red or blue side of the eMSTO, nor any obvious difference in the properties of binaries across the eMSTO, so the present data are inconclusive. We will have to wait for *Gaia* DR4 and LSST-Rubin data to be able to further test this idea.

3.3. Split main sequences

Split MSs were first discovered in clusters belonging to the Magellanic Clouds (Milone et al. 2013) and only later found in the Milky Way (Cordoni et al. 2018). Different explanations were explored, but it is now clear that stars belonging to the two split sequences have different rotation (D'Antona et al. 2015; Dupree et al. 2017; Sun et al. 2019), with the slow rotators on the blue sequence and the fast ones on the red sequence. We identified the split MS visually in the CMD of clusters in our sample and found six clusters with a clearly split MS (namely, NGC 2287, NGC 2301, NGC 2422, NGC 2516, NGC 3766, NGC 6716); to this we added NGC 3532, which we

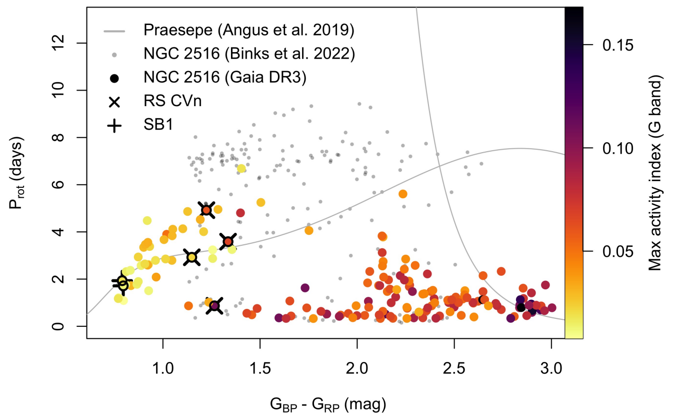

Fig. 7. Lower MS of NGC 2516. Rotation periods from Binks et al. (2022, gray points) and our work (colored points) are compared to the Praesepe period–age relation by Angus et al. (2019, gray lines). The position of confirmed binaries in our catalog is marked by crosses. The activity index, $A_{\rm max}$, is described in detail in Appendix B.3.

classify as eMSTO, but in the literature it has also been classified as a splitMS and an eMSTO (Cordoni et al. 2024). To our knowledge, only NGC 2287 and 2422 were previously reported in the literature besides NGC 3532. We also found 16 clusters with more uncertain hints of a double MS, none of which was previously reported, to our knowledge. In Appendix E.3 we present three examples, sorted by decreasing age.

We suggest, judging from clusters with a good sample of vbroad measurements, that the split MS is the natural continuation of an eMSTO in lower mass clusters. The split MS in our sample always appear above the transition from radiative to convective cores, i.e., the Kraft break (Kraft 1967). The age range of clusters with a split MS is contained into the one of eMSTOs. We could thus say that split MSs and eMSTOs are just two manifestations of the same physical phenomenon (see also Sun et al. 2019). The only exception could be NGC 2422, which appears to have a clear split MS but a very narrow eMSTO (if any). However, this is also the youngest cluster in our sample, so it is expected to have a narrower eMSTO, given the relation between eMSTO photometric spread and age (see previous section). We note that the masses of clusters hosting split MSs are also mostly higher than 1000 $M_{\odot}$, suggesting that cluster mass is an important driving factor, similarly to the case of eMSTO. Finally, we explored the confirmed binary stars in the mentioned clusters: there were very few in the split MS region (from 1 to 4, depending on the cluster). We did not notice any preference for binaries to lie on one sequence or the other, nor any preference for a specific type of binary or binary period (see also Kamann et al. 2021).

3.4. Lower main sequence

Rotation periods in *Gaia* DR2 and DR3 are mostly measured for stars on the lower MS, where the confusion with other types of variable stars is minimized. Stellar rotation changes with cluster age, as low-mass stars slow down because of magnetic braking (see Angus et al. 2019, and references therein). However, young clusters with bimodal distributions of rotational periods were found, especially among T-Tauri stars – for example in the ONC cluster (Attridge & Herbst 1992), NGC 2264 (Lamm et al. 2005), IC 348, and NGC 2362 (Landin et al. 2021) – but also at

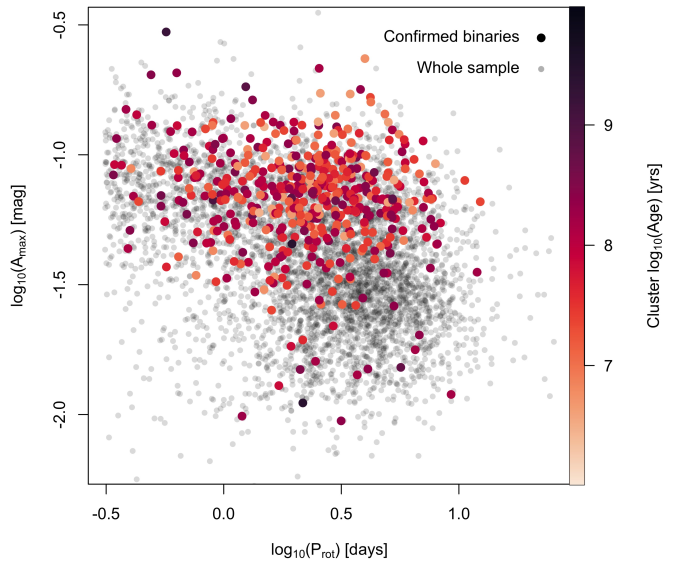

Fig. 8. The period-activity diagram for the whole sample of stars in the lower MS (gray points) and the confirmed binaries (colored points).

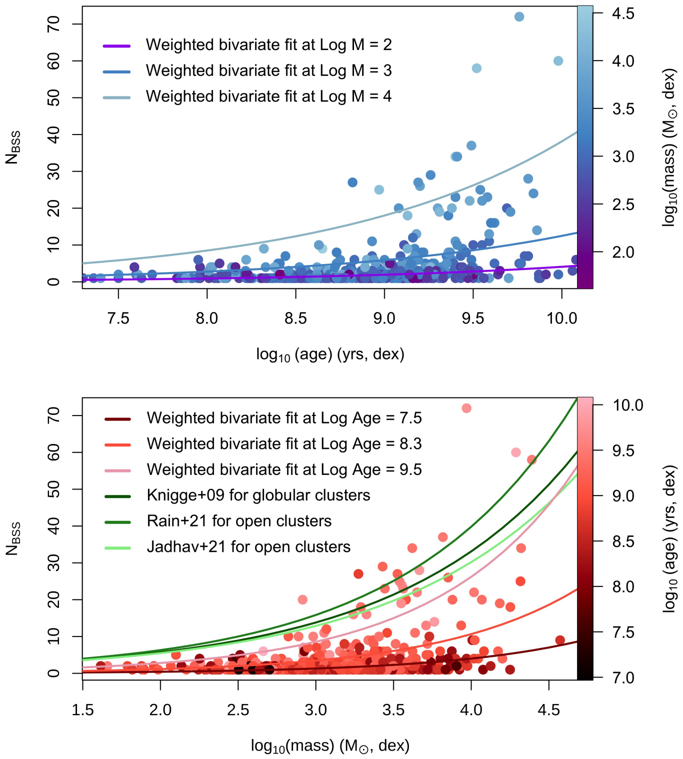

Fig. 9. Total number of BSSs per cluster as a function of cluster age (top panel) and mass (bottom panel). In the two panels, data points are color-coded by cluster mass and age, respectively. Previous literature efforts to model the behavior as a function of mass by Knigge et al. (2009), Jadhav & Subramaniam (2021), and Rain et al. (2021) are plotted in shades of green, as annotated. Our own bivariate fit is plotted in the top panel at fixed $\log M = 2$, 3, and 4 and in the bottom panel at fixed $\log A = 7$, 8.3, and 9.5, on the same color-scale as the data points.

slightly older ages (Bouvier et al. 2014). While slow rotators are well described by gyrochronology models, fast rotators are not. A possible explanation is related to the effect of binary companions or O and B stars' radiation on the disks. These reduce or destroy the disk, which may become less able to lock with the star and to slow it down (Bouvier et al. 1993; Cuello et al. 2025).

A very interesting case is NGC 2516, which shows a clear bifurcation (or at the very least a spread) between slow and fast rotators in the pre-MS stars (Fig. 7). We also notice a possible bifurcation at higher masses in the MS, i.e., bluer than G_{BP}–G_{RP} = 1.5 mag, in the region immediately below the structural transition between stars with convective and radiative cores on the MS (≃1.1–1.3 $M_{\odot}$). NGC 2516 is one of the few clusters in which the whole MS is mapped with both rotation periods and `vbroad`, and it also shows a distinct eMSTO and split MS above the transition region and immediately below the eMSTO (see also Sects. 3.2 and 3.3). As such, it contains in itself examples of all the bimodalities and spreads discussed in the literature and above. This continuity of properties across the entire range of masses suggests a unifying explanation. One possibility, mentioned above, lies in the role of star–disk interactions.

In an attempt to test the idea that binaries are the underlying cause of the rotation bimodality, for example by disturbing the protostellar disks, in Fig. 8 we plot the eight confirmed binaries in NGC 2516, which have both a rotational period and an activity index measurement. The six redder stars are all classified by the *Gaia* classifier as RS CVn types, while the two bluer ones are SB1 stars with 0.5 and 8.1 day orbital periods (i.e., different from their rotational periods, which are around 1.7 and 1.9 days). We note that five of the binaries seem to lie on the fast rotating sequence. However, if we try to generalize this finding using all the clusters in our sample, we encounter some difficulty. Certainly, in clusters above ≃300 Myr there is no particular tendency of binaries to be faster rotators.

In Fig. 8 we show the period-activity diagram for our sample of members with `prot`. Thanks to *Gaia* DR2, it was possible to identify a population of low-activity fast rotators (Lanzafame et al. 2018, 2019), which were only found in very small numbers previously (Messina 2008; Iwanek et al. 2019). It was suggested that this region is populated by binaries, but Lanzafame et al. (2019) proposed that it is a particular phase of the normal evolution of fast-rotating stars. Few cluster members occupy this region, which contains only two binaries, one RS CVn, and one astrometric binary with a period of 616 days. The overall `prot` distribution of binary stars appears very similar to that of the entire sample. On the contrary, binaries tend to cluster in the region of higher activity, unlike the rest of the stars (see also Lanzafame et al. 2018, 2019). With our sample we can add that binaries belonging to old clusters tend to be more spread out, especially in terms of activity index, while binaries in younger clusters tend to be more concentrated toward high activity levels. The binaries in this sample are mostly spectroscopic (SB1 and SB2) and eclipsing. There are also several BY Draconis and RS CVn variables.

3.5. Blue stragglers

Blue straggler stars (BSSs) were discovered in M 3 by Sandage (1953) as stars bluer and brighter than the TO (see also Bailyn 1995). Since then, they have been found in most star clusters and in the field. They are thought to be the result of binary interactions such as mass transfer, stellar mergers, and stellar collisions (McCrea 1964; Hills & Day 1976). Such processes can spin up stars for a certain amount of time, and some BSSs have indeed been found to rotate fast in open and globular clusters (e.g., Lovisi et al. 2010; Leiner et al. 2018). A study based on *Gaia* DR2 and astrometric quality indicators sensitive to binarity suggested that BSSs have the highest fractions of unresolved binaries in the CMD, compatible with up to 100% of them (Belokurov et al. 2020). Indeed, several open clusters were carefully searched for RV variability in the past (see, e.g., Mathieu & Geller 2009; Gosnell et al. 2015; Geller et al. 2015), with about 75–80% of binaries found in the BSS population with periods on the order of 1000 days. A few eclipsing binaries with shorter periods (≲100 days) were also found among candidate BSSs (Arentoft et al. 2007; Kaluzny et al. 2014; Luo 2015; Joshi et al. 2020; Rao et al. 2022). Compact companions to BSSs were found by several authors (e.g., Gosnell et al. 2014, 2015; Subramaniam et al. 2016; Sindhu et al. 2019; Jadhav et al. 2021; Rao et al. 2022), further supporting the idea that binary interactions are an important formation channel, which is dominant in open clusters (Mathieu & Pols 2025).

We relied on the BSS catalogs by Jadhav & Subramaniam (2021), Rain et al. (2021), Li et al. (2023)[4], and Qin et al. (2026), but we manually identified 449 additional BSSs or candidate BSSs (129 with rotation information) with no literature counterpart. Our final sample contains 1932 BSSs (361 with rotation information). As shown in Fig. 9, the total number of BSSs per cluster increases with age (as previously noted by Ahumada & Lapasset 2007; Rain et al. 2021; Leiner & Geller 2021; Li et al. 2023; Cui et al. 2025). Our youngest clusters with BSSs are about 30 Myr old, i.e., younger than the 100 Myr reported in the cited studies[5]. We also observe that the number of BSSs increases with cluster mass, as noted previously for both open and globular clusters (Knigge et al. 2009; Jadhav & Subramaniam 2021; Rain et al. 2021). With our simultaneous mass and age determinations, we note that both need to be high – i.e., $M \gtrsim 1000\,M_\odot$ and age ≳ 500 Myr, respectively – to have more than ≃5–10 BSSs in a given cluster. We computed a weighted bivariate fit that appears to capture the observed behavior more closely compared to previous univariate fits (Rain et al. 2021; Jadhav & Subramaniam 2021),

$$N_{\rm BSS} = 10^{-3.62(\pm0.26)+0.48(\pm0.03)\,{\rm Log}M+0.33(\pm0.03)\,{\rm Log}A},$$

where M and A are mass and age, respectively, and $N_{\rm BSS}$ is the number of BSSs in each cluster. The fits are reported in Fig. 9.

In Fig. 4 we examine the overall `vbroad` distribution of 77 BSSs. We observe that among the studied populations, BSSs differ the most from the MS sample. Their distribution has an irregular shape, which could be an indication of an underlying multimodality or just the result of the relatively smaller sample. We suspect that the main peak at ≃50 km s^{-1} could be at least in part caused by unresolved SB2, but the excess of fast rotators at ≃150 km s^{-1} is certainly not made by unresolved binaries. We find a larger median `ruwe`[6] of 1.14 in the BSS rotating slower than 100 km s^{-1} than in the faster ones, where we find only 0.98. This could be taken as supporting evidence that the ≃50 km s^{-1} peak is dominated by astrometric binaries, but needs confirmation. To compare with globular clusters, we note that Ferraro et al. (2023) found 40% of the BSS rotating faster than >40 km s^{-1} in loose clusters, while only 4% were found in high-density globular clusters. Our fraction of BSSs in open clusters rotating faster than 40 km s^{-1} is 76%. This makes sense if we consider that all open clusters are certainly loose compared to globular clusters. In the case of globular clusters, this was interpreted as evidence that BSSs are still forming in loose clusters. This could also be the case in open clusters; i.e., fast-rotating BSSs would be recently formed, but with the caveat that we also have some more massive BSSs in our sample, which could spin down more slowly than low-mass ones (see Leiner et al. 2018, for FGK type BSS) and thus should not be interpreted as having formed more recently.

Finally, we report that 97 BSSs are found to be binaries or suspected binaries in our sample (i.e., about 6%). They are mostly classified as eclipsing binaries, but there are also some SB1 and SB2 types, and some might have hot companions, judging from their UV excess (Jackim et al. 2024). A few are classified in *Gaia* with acceleration solutions, which means that the period must be comparable to or longer than the 34 months covered in DR3. The few that have period determinations are always below 4 days; only one is 233 days. Four stars are contact binaries, and one may be in a common envelope phase. These short period binaries are not common among BSSs, which is compatible with the small fraction found here. They may be indicative of case A mass transfer[7], with low-mass MS companions expected (Rao et al. 2022; Sandquist et al. 2003). Longer period BSS binaries – i.e., about 75–80% in open clusters in the literature (Mathieu & Pols 2025) – often have WD-like companions and would more likely be the result of case B or C mass transfer, but for the moment they are out of reach for *Gaia*.

3.6. Red giants and subgiants

Fast-rotating (>10 km s^{-1}) red giant branch stars (RGBs) are rare and are thought to be byproducts of binary interactions (Carlberg et al. 2011; Gaulme et al. 2020; Patton et al. 2024), because the expanded envelopes of giant stars lead to low projected rotational speed, generally <5 km s^{-1}. Among the interactions with (sub)stellar companions that can transfer angular momentum are tidal synchronization, mass transfer, and mergers. Thus, in some cases we may be able to observe a companion, while in the case of mergers the star will be single (see, e.g., Carlberg et al. 2011, and references therein).

We selected a sample of rotationally characterized red giants and subgiant branch stars (SGBs) by visually inspecting the CMD of each cluster with at least one `vbroad` or `vsini` measurement. We used BaSTI isochrones (Hidalgo et al. 2018) to guide the eye in the case of less populated clusters, but the candidates were selected only when the RGB and SGB sequences were clearly visible in the CMD, and we did not use the isochrones in the actual selection (see, e.g., Ramos et al. 2024). Our final sample of rotationally characterized red giants and subgiants contains 2369 and 85 stars, respectively, which are displayed in the top panel of Fig. 10. Even considering the limitations of the *Gaia* `vbroad` measurements (cyan region in Fig. 10), our sample overlaps the one of field giants by Carlberg et al. (2011). The difference in spectral resolution between the two samples can be appreciated, because the Carlberg et al. (2011) sample reaches down to a broadening of almost 0 km s^{-1} while the *Gaia* one barely reaches 5 km s^{-1}. We also observe that the RGB distribution is different from the dwarfs samples in Figs. 4 and 5. The `vbroad` distribution of RGB and SGB stars is shown in Fig. 11 and is very strongly

[4] We were not able to use the new BSS identified by Cui et al. (2025) because the authors did not provide the full list.

[5] Negueruela et al. (2023) found that blue supergiants in young clusters are more massive than predicted from single star evolution, and thus there could be BSSs in even younger clusters.

[6] The renormalized unit weight error in the *Gaia* catalog indicates extra noise in the astrometric solution for a given source, which can also be caused by binary companion, among other things.

[7] Case A mass transfer happens when the donor is on the MS, while case B happens on the RGB, and case C on the asymptotic giant branch.

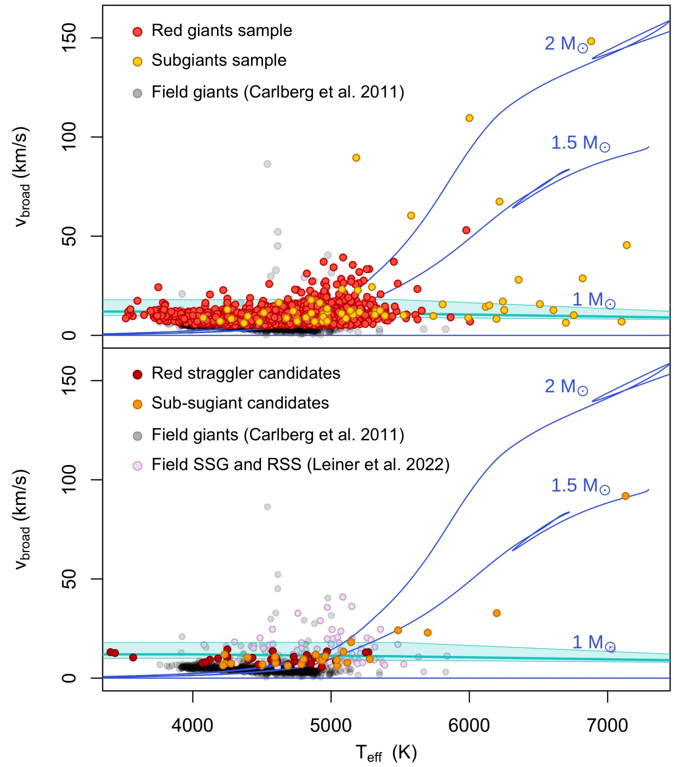

Fig. 10. Top panel. RGB (red points) and SGB (yellow points) samples are compared with the sample of field giants by Carlberg et al. (2011) in the $T_{\rm eff}$ vbroad plane. Bottom panel. Same as the top panel but for the RSS (dark red points) and SSG (orange points) candidates. Here, we also plot the *Gaia* measurements for the sample of field SSGs and RSSs (thistle points) by Leiner et al. (2022). In both panels, the cyan line and shaded area represent the region where *Gaia* vbroad starts to be overestimated, with its uncertainty range (Frémat et al. 2023, Table 2). The MIST rotational models (Choi et al. 2016) with $\Omega_{\rm ZAMS}/\Omega_{\rm crit} = 0.4$ are also plotted in blue for reference.

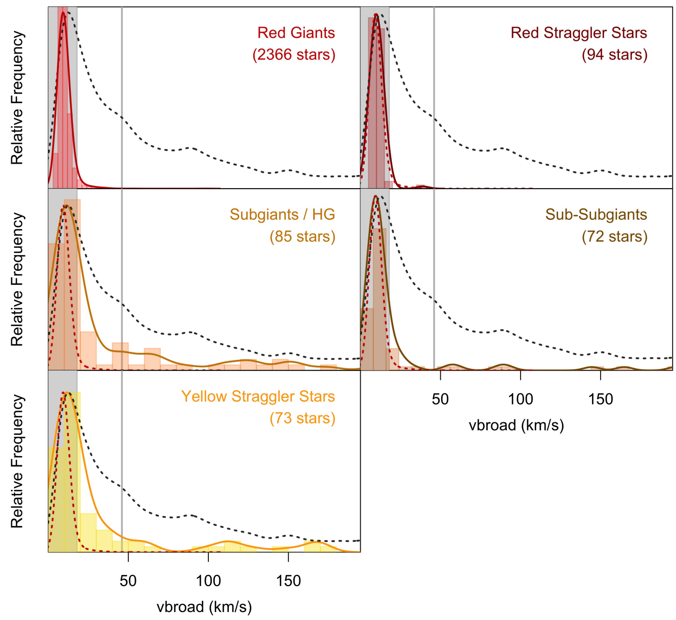

Fig. 11. Similar to Fig. 4 but for the samples of giants, as annotated.

peaked at 9.6 ± 2.6 km s^{-1}. This is determined by the RVS resolution limits (Frémat et al. 2023) and does not represent the intrinsic rotation of the stars; thus, we focused our analysis on the long tail of fast-rotating stars, reaching 98.3 km s^{-1}.

We selected fast-rotating giants as those being more than 3σ faster than the average, i.e., vbroad > 17.4. We obtained a sample of 79 stars (4%), which is comparable with previous findings in the literature (Carlberg et al. 2011). Of these, 26 (33%) are flagged as variable or suspect variable stars (see Appendix D.1) and nine (11%) are flagged as binary or suspect binaries (see Appendix D.2). For reference, the whole giant sample has a variable star fraction of 14% and binary fraction of 11%. Most classifications are uncertain or generic (long period, rotational). Notably, there are three fast-rotating giants classified by *Gaia* as RS CVn, but not parameterized; five are classified by *Gaia* or spectroscopic surveys as SB1; and two are classified as eclipsing binaries. The available periods range from 8 to >10^4 d, with a median of about 100 d. Because our binary characterization may be biased and incomplete, we also tried another approach. An analysis by Patton et al. (2024) employed indirect criteria such as velocity spreads of APOGEE data and ruwe in *Gaia* to estimate the number of binaries among fast-rotating giants in APOGEE, finding striking fractions of 75% or higher. Our giant sample has a median ruwe = 1.01 ± 0.12. Therefore, an appropriate threshold would be 1.37, which is different from the value of 1.2 used by Patton et al. (2024). In any case, using the two thresholds, we find 6% and 11% of suspect binaries, respectively, which is compatible with the fraction computed over the entire giant sample; i.e., 5% and 12%, respectively.

We note that the saturation threshold of *Gaia* DR3 vbroad prevents us from separating the intermediate rotators (or anomalous rotators, with 5–10 km s^{-1}, Tayar et al. 2015) from the slow-rotating giants. This could be one of the causes of the tension between our results on the binary fractions and those by Patton et al. (2024). Thus, a possible interpretation is that our sample of fast rotators is dominated by mergers and that binaries may dominate in the intermediate sample that we cannot discern with our data. Another possibility is that, considering that mergers should be more common in the cluster environment than in the field, our cluster sample of giants is intrinsically different from the field samples in the literature, containing relatively more mergers and therefore fewer binaries.

3.7. *Red stragglers and sub-subgiants*

Red stragglers (RSSs) and sub-subgiants (SSGs) occupy a region of the CMD that is, respectively, redder than the red giant branch or fainter than the sub-giant branch. The first two SSGs were discovered in M 67 by Mathieu et al. (2003). Several years later a census of the 65 known SSGs and RSSs in open and globular clusters was published by Geller et al. (2017), and a sample of 448 RSSs and SSGs in the field population was presented by Leiner et al. (2022). Several of these stars are X-ray emitters, binaries, variables, or spotted, and/or they display H_α emission. Moreover, RS CVn variables are found in the known samples (Dixon et al. 2025). According to Leiner et al. (2022), prot peaks at about five days in the field sample, with a long tail reaching tens of days. The distributions of prot for field and cluster SSGs appear compatible with each other. Two different explanations were put forward in the above cited studies for their noncanonical position in the CMD. The favored one is that SSGs and RSSs are spun-up by binary interactions and develop magnetic fields, and so they appear fainter and redder because of spots and possible radius inflation. The second is that they are undergoing important mass-transfer episodes which bring them temporarily out of equilibrium.

We selected 158 (rotationally characterized) candidate SSGs and RSSs from individual-cluster CMDs. When the RGB and SGB were sufficiently populated, we selected our candidates as 3σ outliers. When the RGB and SGB were scarcely populated, we relied on BaSTI isochrones (Hidalgo et al. 2018), and thus on cluster parameters, to guide our selections. Unfortunately, we have no candidates in common with Geller et al. (2017), because their sources are too faint to be rotationally characterized in *Gaia* DR3. The sample is presented in Fig. 10 (bottom panel), where it is compared with the distribution of field giants by Carlberg et al. (2011) and the *Gaia* parameters of field SSGs and RSSs by Leiner et al. (2022). The fraction of fast-rotating stars in our sample agrees well with the field sample by Leiner et al. (2022). If we cross-match the field sample with *Gaia*, we find 5% of the stars have `vbroad` > 17.4 km s^{-1}, while if we do the same with our sample, we find 8%. Moreover, it was found that `prot` tends to increase from a SSG to a RSS (Leiner et al. 2022), which is compatible with stellar evolution expectations. Our sample confirms this finding, as can be seen from Fig. 10 but also from Fig. 11; the RSS `vbroad` distribution is more peaked and has virtually no tail toward higher values, unlike the SSG sample.

Concerning the possible binary nature of our candidates, we note that the entire sample of RSSs and SSGs has a fraction of variable stars of 7% and of binary stars of 17%. These figures are higher than, but comparable to those of the combined RGB and SGB sample, i.e., 14% and 11%. The types of binaries found among RSS and SSG candidates are typically SB1 spectroscopic binaries. The only fast rotating RSS is reported by *Gaia* DR3 as an RS CVn type, but is not parameterized. Previous reports by the ATLAS survey (Heinze et al. 2018) also classify it as a possible eclipsing binary with a sinusoidal light curve. The `ruwe` of these RSS and SSG candidates is indistinguishable from that of normal giants. If `ruwe` > 1.37 was taken as an indirect indication of binarity, it would suggest a binary fraction of 14%. In conclusion, with the data in hand, we can only report a slight increase (17% versus 11%) in the binary discovery fraction of RSSs and SSGs with respect to the normal red giants.

3.8. Yellow-straggler candidates

Evolved BSSs should appear brighter than the sub-giant branch and redder than BSSs. In the literature they are thus called either red or yellow straggler stars (Sales Silva et al. 2014). To avoid any confusion with the RSS (Sect. 3.7), we adopted the term yellow straggler star (YSS). Unfortunately, the region where evolved BSSs are expected to lie also hosts evolved binaries of various kinds, and the continuation of the equal-mass binary sequence (Sect. 3.1). Indeed, several of the known YSSs have shown A-type companions, identified by the presence of Balmer lines and veiling in the blue spectral regions (Sales Silva et al. 2014; da Silveira et al. 2018; Martinez et al. 2020; Rani et al. 2023). In these cases, it is believed that the yellow color is driven by the contamination of the blue companion, making YSSs bluer than RGB stars, but still redder than the typical BSS. For all these reasons, we refer to our YSS sample as YSS candidates in the following.

We relied on the YSSs selected by Rain et al. (2021) and Li et al. (2023). We further selected new YSS candidates as stars redder than the TO, bluer than the RGB, and brighter than the SGB. We only used clusters with sufficiently populated sequences and we did not use isochrones to compensate for the lack of data. Our YSS-candidate sample counts 134 stars, doubling the literature samples. In Fig. 11 we compare their `vbroad` distribution with that of other samples of giants and subgiants, which are discussed above. The YSS candidates rotating faster than 17.4 km s^{-1} (see Sect. 3.6) are ≃38%, compared to 4% for normal giants. We found 23 potential or confirmed binaries in the YSS sample (17%). Almost all are classified as type SB1 (Pourbaix et al. 2004; Gavras et al. 2023), and a few are classified as eclipsing binaries or RS CVn in *Gaia* DR3, but they are not parameterized. One has UV excess in GALEX (Jackim et al. 2024). When available, periods range from one to more than 1000 days. Only one of the binaries is also rotating faster than 17.4 km s^{-1}. If all the rotating YSS candidates are assumed to be binaries, this would bring the (still uncorrected) binary fraction of YSS candidates to ≃46%. This result supports the idea that this portion of the CMD is dominated by binaries and their byproducts. Unfortunately, as mentioned, we cannot cleanly separate YSSs from other types of binaries that are known to populate this region.

4. Summary and conclusions

In this work, we selected and characterized a sample of more than 700 000 members of almost 6000 open clusters. We employed *Gaia* DR3 information of stellar rotation – both from the width of RVS spectra and from the light curves of spotted rotating stars – to study the behavior of various stellar samples across the CMD.

Our main results can be summarized as follows:

- We classified a large number of stars in the MS and binMS and found a statistically significant excess of rotation in the binMS sample. The binMS sample contains a similar proportion of binaries to the MS (≃6% compared to 7%). To clean the samples from abnormally fast rotating stars, we produced a sample of about 100 new candidate BLs, which we make available for further study.
- We significantly increased the number of clusters with an eMSTO or a split the MS compared to the previous literature, bringing it to about 100, plus a few hundred clusters with suspected complex TO regions. We support the idea that the photometric spread is not entirely explained by the `vbroad` spread, as previously suggested in the literature. We further observe that most clusters with a mass higher than about 1000 M$_\odot$ display an eMSTO. We also notice that the spread in `vbroad` seems to decrease with age for older clusters, in apparent contradiction with the photometric spread, which increases with age. This may not be a true inconsistency, but it needs to be explored with the help of models.
- In the lower main sequence, we observe that the confirmed binaries can be slow or fast rotators, but most of them have high activity levels, as measured from the amplitude of the light curve and previously noted in the literature. We further note that binaries in older clusters extend to lower activity levels compared to younger clusters.
- We discovered several hundred new stars belonging to various exotic populations. In the case of BSSs, we obtained a combined sample of new discoveries and literature detections to almost 2000 BSSs. We observe that the clusters with more than 5–10 BSSs generally have both high masses ($\gtrsim$1000 M$_\odot$) and old ages ($\gtrsim$1 Gyr), and we provide a bivariate fit that reproduces the behavior better than previous univariate fits. The `vbroad` distribution significantly differs from the one of MS stars and presents an irregular shape. The fraction of stars rotating more than 40 km s^{-1} is about

75%. We found several binaries with relatively short periods among BSSs (about 6%), which is compatible with previous literature studies. Longer period binaries are for the moment out of reach of *Gaia*.
- Among red giants and subgiants we found a small group of abnormally fast rotators (about 4%), compatible with previous findings for field stars, while the rest of the sample displays the expected rotational behavior. These fast rotating stars can only be the result of recent binary interactions, and indeed they display higher proportions of known binaries than the slowly rotating giants.
- The samples of YSS candidates, RSSs, and SSGs display more prominent tails of fast rotating stars compared to the RGB sample. The percentage of binaries in these populations is slightly higher than in the RGB sample. About 33% of fast-rotating YSS candidates are binaries.

Our bird's-eye exploration of the properties of rotating stars in open clusters revealed a few interesting new facts that are worth following up with dedicated studies. We hope that this new and increased sample will help solve some of the long-standing problems in the field. The future is bright. On one hand, the spectroscopic surveys already contain a treasure trove of `vbroad` measurements that only awaits to be explored in a synergic way, similarly to what has been done in projects such as the Survey of Surveys (Tsantaki et al. 2022; Turchi et al. 2025). On the other hand, the upcoming *Gaia* DR4 data are expected to significantly improve the quantity and quality of the measurements, and especially the inventory of binary stars, which are expected to be closely linked with stellar rotation. LSST–Rubin will additionally soon provide an overwhelming amount of high-quality light curves (Ivezić et al. 2019).

Data availability

The catalogs described in Tables 1 and 2 are available at the CDS via `https://cdsarc.cds.unistra.fr/viz-bin/cat/J/A+A/711/A67`

Acknowledgements. We would like to thank the following colleagues for useful comments and suggestions: Eleonora Bianchi, Katia Biazzo, Santi Cassisi, Michele Fabrizio, Yves Frémat, Alessandro Lanzafame, Emily Leiner, Bob Mathieu, Frédéric Royer, Claudia Toci. Co-funded by the European Union (ERC-2022-AdG, *"StarDance: the non-canonical evolution of stars in clusters"*, Grant Agreement 101093572, PI: E. Pancino). Views and opinions expressed are however those of the author(s) only and do not necessarily reflect those of the European Union or the European Research Council. Neither the European Union nor the granting authority can be held responsible for them. EP acknowledges financial support from PRIN-MIUR-22: CHRONOS: adjusting the clock(s) to unveil the CHRONO-chemo-dynamical Structure of the Galaxy" (PI: S. Cassisi) funded by the European Union – Next Generation EU. VVJ acknowledges support through grant 26-21774S from the Czech Grant Agency. This work has made use of data from the European Space Agency (ESA) mission Gaia (`https://www.cosmos.esa.int/gaia`), processed by the Gaia Data Processing and Analysis Consortium (DPAC, `https://www.cosmos.esa.int/web/gaia/dpac/consortium`). Funding for the DPAC has been provided by national institutions, in particular the institutions participating in the Gaia Multilateral Agreement. Funding for the Sloan Digital Sky Survey IV has been provided by the Alfred P. Sloan Foundation, the U.S. Department of Energy Office of Science, and the Participating Institutions. SDSS-IV acknowledges support and resources from the Center for High Performance Computing at the University of Utah. Guoshoujing Telescope (the Large Sky Area Multi-Object Fiber Spectroscopic Telescope LAMOST) is a National Major Scientific Project built by the Chinese Academy of Sciences. Funding for the project has been provided by the National Development and Reform Commission. LAMOST is operated and managed by the National Astronomical Observatories, Chinese Academy of Sciences. Most of the plotting and data analysis was carried out using R (R Core Team 2017; Dowle & Srinivasan 2017). This research has made use of the SIMBAD database (Wenger et al. 2000) and the VizieR catalogue access tool (Ochsenbein et al. 2000), both operated at CDS, Strasbourg, France. Preliminary data exploration relied on TopCat (Taylor 2005).

References

Abdurro'uf, Accetta, K., Aerts, C., et al. 2022, ApJS, 259, 35
Ahumada, J. A., & Lapasset, E. 2007, A&A, 463, 789
Ahumada, R., Prieto, C. A., Almeida, A., et al. 2020, ApJS, 249, 3
Alexander, J. S., & Albrow, M. D. 2025, MNRAS, 536, 471
Andrae, R., Rix, H.-W., & Chandra, V. 2023, ApJS, 267, 8
Andrew, S., Penoyre, Z., Belokurov, V., Evans, N. W., & Oh, S. 2022, MNRAS, 516, 3661
Angus, R., Morton, T. D., Foreman-Mackey, D., et al. 2019, AJ, 158, 173
Arentoft, T., De Ridder, J., Grundahl, F., et al. 2007, A&A, 465, 965
Attridge, J. M., & Herbst, W. 1992, ApJ, 398, L61
Babusiaux, C., Fabricius, C., Khanna, S., et al. 2023, A&A, 674, A32
Bailer-Jones, C. A. L., Rybizki, J., Fouesneau, M., Demleitner, M., & Andrae, R. 2021, AJ, 161, 147
Bailyn, C. D. 1995, ARA&A, 33, 133
Bastian, N., Kamann, S., Cabrera-Ziri, I., et al. 2018, MNRAS, 480, 3739
Bastian, N., Kamann, S., Amard, L., et al. 2020, MNRAS, 495, 1978
Belokurov, V., Penoyre, Z., Oh, S., et al. 2020, MNRAS, 496, 1922
Berger, T. A., Huber, D., van Saders, J. L., et al. 2020, AJ, 159, 280
Bertelli, G., Nasi, E., Girardi, L., et al. 2003, AJ, 125, 770
Binks, A. S., Jeffries, R. D., Sacco, G. G., et al. 2022, MNRAS, 513, 5727
Birko, D., Zwitter, T., Grebel, E. K., et al. 2019, AJ, 158, 155
Blomme, R., Frémat, Y., Sartoretti, P., et al. 2023, A&A, 674, A7
Boin, T., Casamiquela, L., Haywood, M., et al. 2026, A&A, 708, A215
Bouvier, J., Cabrit, S., Fernandez, M., Martin, E. L., & Matthews, J. M. 1993, A&A, 272, 176
Bouvier, J., Matt, S. P., Mohanty, S., et al. 2014, in Protostars and Planets VI, eds. H. Beuther, R. S. Klessen, C. P. Dullemond, T. Henning, 433
Buder, S., Asplund, M., Duong, L., et al. 2018, MNRAS, 478, 4513
Buder, S., Kos, J., Wang, X. E., et al. 2025, PASA, 42, e051
Cantat-Gaudin, T., & Anders, F. 2020, A&A, 633, A99
Cantat-Gaudin, T., Jordi, C., Vallenari, A., et al. 2018a, A&A, 618, A93
Cantat-Gaudin, T., Vallenari, A., Sordo, R., et al. 2018b, A&A, 615, A49
Cantat-Gaudin, T., Anders, F., Castro-Ginard, A., et al. 2020, A&A, 640, A1
Carlberg, J. K., Majewski, S. R., Patterson, R. J., et al. 2011, ApJ, 732, 39
Castro-Ginard, A., Jordi, C., Luri, X., et al. 2018, A&A, 618, A59
Castro-Ginard, A., Jordi, C., Luri, X., Cantat-Gaudin, T., & Balaguer-Núñez, L. 2019, A&A, 627, A35
Castro-Ginard, A., McMillan, P. J., Luri, X., et al. 2021, A&A, 652, A162
Castro-Ginard, A., Jordi, C., Luri, X., et al. 2022, A&A, 661, A118
Cavallo, L., Spina, L., Carraro, G., et al. 2024, AJ, 167, 12
Chen, X., Wang, S., Deng, L., et al. 2020, ApJS, 249, 18
Choi, J., Dotter, A., Conroy, C., et al. 2016, ApJ, 823, 102
Clementini, G., Ripepi, V., Garofalo, A., et al. 2023, A&A, 674, A18
Cordoni, G., Milone, A. P., Marino, A. F., et al. 2018, ApJ, 869, 139
Cordoni, G., Casagrande, L., Yu, J., et al. 2024, MNRAS, 532, 1547
Correnti, M., Goudfrooij, P., Bellini, A., Kalirai, J. S., & Puzia, T. H. 2017, MNRAS, 467, 3628
Cropper, M., Katz, D., Sartoretti, P., et al. 2018, A&A, 616, A5
Cuello, N., Alaguero, A., & Poblete, P. P. 2025, Symmetry, 17, 344
Cui, Q., He, Z., Deng, S., et al. 2025, AJ, 169, 219
da Silveira, M. D., Pereira, C. B., & Drake, N. A. 2018, MNRAS, 476, 4907
D'Antona, F., Di Criscienzo, M., Decressin, T., et al. 2015, MNRAS, 453, 2637
D'Antona, F., Milone, A. P., Tailo, M., et al. 2017, Nat. Astron., 1, 0186
Deleuil, M., Aigrain, S., Moutou, C., et al. 2018, A&A, 619, A97
Deng, Y.-Y., & Li, Z.-M. 2024, Res. Astron. Astrophys., 24, 065004
Dias, W. S., Alessi, B. S., Moitinho, A., & Lépine, J. R. D. 2002, A&A, 389, 871
Dias, W. S., Monteiro, H., Moitinho, A., et al. 2021, MNRAS, 504, 356
Distefano, E., Lanzafame, A. C., Brugaletta, E., et al. 2023, A&A, 674, A20
Dixon, D., Stassun, K. G., Mathieu, R. D., Tayar, J., & Cao, L. 2025, AJ, 169, 309
Dowle, M., & Srinivasan, A. 2017, data.table: Extension of 'data.frame', r package version 1.10.4-3
Doyle, A. P., Davies, G. R., Smalley, B., Chaplin, W. J., & Elsworth, Y. 2014, MNRAS, 444, 3592
Dupree, A. K., Dotter, A., Johnson, C. I., et al. 2017, ApJ, 846, L1
Duquennoy, A., & Mayor, M. 1991, A&A, 248, 485
El-Badry, K., Ting, Y.-S., Rix, H.-W., et al. 2018, MNRAS, 476, 528
Eyer, L., Audard, M., Holl, B., et al. 2023, A&A, 674, A13
Ferraro, F. R., Mucciarelli, A., Lanzoni, B., et al. 2023, Nat. Commun., 14, 2584
Ferreira, F. A., Santos, J. F. C., Corradi, W. J. B., Maia, F. F. S., & Angelo, M. S. 2019, MNRAS, 483, 5508

Ferreira, F. A., Corradi, W. J. B., Maia, F. F. S., Angelo, M. S., & Santos, J. F. C., Jr. 2020, MNRAS, 496, 2021
Ferreira, F. A., Corradi, W. J. B., Maia, F. F. S., Angelo, M. S., & Santos, J. F. C., Jr. 2021, MNRAS, 502, L90
Fisher, J., Schröder, K.-P., & Smith, R. C. 2005, MNRAS, 361, 495
Fouesneau, M., Frémat, Y., Andrae, R., et al. 2023, A&A, 674, A28
Frémat, Y. 2024, in EES2023: Proceedings of the Evry Schatzman School, eds. C. Babusiaux, & C. Reylé, 59
Frémat, Y., Royer, F., Marchal, O., et al. 2023, A&A, 674, A8
Fu, X., Bragaglia, A., Liu, C., et al. 2022, A&A, 668, A4
Gaia Collaboration (Prusti, T., et al.) 2016, A&A, 595, A1
Gaia Collaboration (Brown, A. G. A., et al.) 2018, A&A, 616, A1
Gaia Collaboration (Arenou, F., et al.) 2023a, A&A, 674, A34
Gaia Collaboration (De Ridder, J., et al.) 2023b, A&A, 674, A36
Gaia Collaboration (Vallenari, A., et al.) 2023c, A&A, 674, A1
Gao, X., Chen, X., Wang, S., & Liu, J. 2025, ApJS, 276, 57
Gaulme, P., Jackiewicz, J., Spada, F., et al. 2020, A&A, 639, A63
Gavras, P., Rimoldini, L., Nienartowicz, K., et al. 2023, A&A, 674, A22
Geller, A. M., Latham, D. W., & Mathieu, R. D. 2015, AJ, 150, 97
Geller, A. M., Leiner, E. M., Bellini, A., et al. 2017, ApJ, 840, 66
Georgy, C., Ekström, S., Eggenberger, P., et al. 2013, A&A, 558, A103
Gilmore, G., Randich, S., Asplund, M., et al. 2012, Messenger, 147, 25
Gomel, R., Mazeh, T., Faigler, S., et al. 2023, A&A, 674, A19
Gosnell, N. M., Mathieu, R. D., Geller, A. M., et al. 2014, ApJ, 783, L8
Gosnell, N. M., Mathieu, R. D., Geller, A. M., et al. 2015, ApJ, 814, 163
Goudfrooij, P., Girardi, L., Kozhurina-Platais, V., et al. 2014, ApJ, 797, 35
Grondin, S. M., Drout, M. R., Nordhaus, J., et al. 2024, ApJ, 976, 102
Halbwachs, J.-L., Pourbaix, D., Arenou, F., et al. 2023, A&A, 674, A9
Hao, C. J., Xu, Y., Wu, Z. Y., et al. 2022, A&A, 660, A4
He, Z.-H., Xu, Y., Hao, C.-J., Wu, Z.-Y., & Li, J.-J. 2021, Res. Astron. Astrophys., 21, 093
Heinze, A. N., Tonry, J. L., Denneau, L., et al. 2018, AJ, 156, 241
Hidalgo, S. L., Pietrinferni, A., Cassisi, S., et al. 2018, ApJ, 856, 125
Hills, J. G., & Day, C. A. 1976, Astrophys. Lett., 17, 87
Hodgkin, S. T., Harrison, D. L., Breedt, E., et al. 2021, A&A, 652, A76
Holl, B., Sozzetti, A., Sahlmann, J., et al. 2023, A&A, 674, A10
Hunt, E. L., & Reffert, S. 2021, A&A, 646, A104
Hunt, E. L., & Reffert, S. 2023, A&A, 673, A114
Hunt, E. L., & Reffert, S. 2024, A&A, 686, A42
Hurley, J. R., Tout, C. A., & Pols, O. R. 2002, MNRAS, 329, 897
Hut, P. 1981, A&A, 99, 126
Ivezić, Ž., Kahn, S. M., Tyson, J. A., et al. 2019, ApJ, 873, 111
Iwanek, P., Soszyński, I., Skowron, J., et al. 2019, ApJ, 879, 114
Iwanek, P., Soszyński, I., Kozłowski, S., et al. 2022, ApJS, 260, 46
Jackim, R., Heyl, J., & Richer, H. 2024, arXiv e-prints [arXiv:2404.07388]
Jadhav, V. V., & Subramaniam, A. 2021, MNRAS, 507, 1699
Jadhav, V. V., Sindhu, N., & Subramaniam, A. 2019, ApJ, 886, 13
Jadhav, V. V., Pandey, S., Subramaniam, A., & Sagar, R. 2021, JApA, 42, 89
Jadhav, V. V., Subramaniam, A., & Sagar, R. 2023, A&A, 676, A47
Jadhav, V. V., Subramaniam, A., & Sagar, R. 2024, A&A, 688, A152
Jadhav, V. V., Rao, K. K., & Reggiani, E. 2026, A&A, 707, A275
Jayasinghe, T., Kochanek, C. S., Stanek, K. Z., et al. 2021, MNRAS, 503, 200
Johnston, C., Aerts, C., Pedersen, M. G., & Bastian, N. 2019, A&A, 632, A74
Jonsson, S., West, J., & Liem Nguyen, V. 2020, in EGU General Assembly Conference Abstracts, EGU General Assembly Conference Abstracts, 19646
Joshi, Y. C., John, A. A., Maurya, J., et al. 2020, MNRAS, 499, 618
Kähler, H. 1999, A&A, 346, 67
Kaluzny, J., Rozyczka, M., Pych, W., & Thompson, I. B. 2014, Acta Astron., 64, 77
Kamann, S., Bastian, N., Usher, C., Cabrera-Ziri, I., & Saracino, S. 2021, MNRAS, 508, 2302
Kamann, S., Saracino, S., Bastian, N., et al. 2023, MNRAS, 518, 1505
Katz, D., Sartoretti, P., Cropper, M., et al. 2019, A&A, 622, A205
Katz, D., Sartoretti, P., Guerrier, A., et al. 2023, A&A, 674, A5
Kharchenko, N. V., Piskunov, A. E., Schilbach, E., Röser, S., & Scholz, R. D. 2013, A&A, 558, A53
Kirk, B., Conroy, K., Prša, A., et al. 2016, AJ, 151, 68
Knigge, C., Leigh, N., & Sills, A. 2009, Nature, 457, 288
Kounkel, M., Covey, K. R., Stassun, K. G., et al. 2021, AJ, 162, 184
Kovalev, M., Zhou, Z., Chen, X., & Han, Z. 2024, MNRAS, 527, 521
Kraft, R. P. 1967, ApJ, 150, 551
Lamm, M. H., Mundt, R., Bailer-Jones, C. A. L., & Herbst, W. 2005, A&A, 430, 1005
Landin, N. R., Chaves, J. K. L., Souza, T. S. M., et al. 2021, in The 20.5th Cambridge Workshop on Cool Stars, Stellar Systems, and the Sun (CS20.5), Cambridge Workshop on Cool Stars, Stellar Systems, and the Sun, 329
Lanzafame, A. C., Distefano, E., Messina, S., et al. 2018, A&A, 616, A16
Lanzafame, A. C., Distefano, E., Barnes, S. A., & Spada, F. 2019, ApJ, 877, 157
Lebzelter, T., Mowlavi, N., Lecoeur-Taibi, I., et al. 2023, A&A, 674, A15
Leiner, E. M., & Geller, A. 2021, ApJ, 908, 229
Leiner, E., Mathieu, R. D., Gosnell, N. M., & Sills, A. 2018, ApJ, 869, L29
Leiner, E., Mathieu, R. D., Vanderburg, A., Gosnell, N. M., & Smith, J. C. 2019, ApJ, 881, 47
Leiner, E. M., Geller, A. M., Gully-Santiago, M. A., Gosnell, N. M., & Tofflemire, B. M. 2022, ApJ, 927, 222
Leiner, E. M., Gosnell, N. M., Geller, A. M., et al. 2025, ApJ, 979, L1
Li, C., Zhong, J., Qin, S., & Chen, L. 2023, A&A, 672, A81
Lovisi, L., Mucciarelli, A., Ferraro, F. R., et al. 2010, ApJ, 719, L121
Luo, Y.-P. 2015, Res. Astron. Astrophys., 15, 733
Mackey, A. D., & Broby Nielsen, P. 2007, MNRAS, 379, 151
Maeder, A., & Meynet, G. 2000, ARA&A, 38, 143
Marrese, P. M., Marinoni, S., Fabrizio, M., & Giuffrida, G. 2017, A&A, 607, A105
Marrese, P. M., Marinoni, S., Fabrizio, M., & Altavilla, G. 2019, A&A, 621, A144
Martinez, C. F., Holanda, N., Pereira, C. B., & Drake, N. A. 2020, MNRAS, 494, 1470
Marton, G., Ábrahám, P., Rimoldini, L., et al. 2023, A&A, 674, A21
Mathieu, R. D., & Geller, A. M. 2009, Nature, 462, 1032
Mathieu, R. D., & Pols, O. R. 2025, ARA&A, 63, 467
Mathieu, R. D., van den Berg, M., Torres, G., et al. 2003, AJ, 125, 246
Mazzola, C. N., Badenes, C., Moe, M., et al. 2020, MNRAS, 499, 1607
McCrea, W. H. 1964, MNRAS, 128, 147
Merle, T., Van Eck, S., Jorissen, A., et al. 2017, A&A, 608, A95
Merle, T., Van der Swaelmen, M., Van Eck, S., et al. 2020, A&A, 635, A155
Mermilliod, J. C., Mayor, M., & Udry, S. 2008, A&A, 485, 303
Mermilliod, J. C., Mayor, M., & Udry, S. 2009, A&A, 498, 949
Messina, S. 2008, A&A, 480, 495
Meynet, G., & Maeder, A. 2002, A&A, 381, L25
Milone, A. P., Piotto, G., Bedin, L. R., et al. 2012, A&A, 540, A16
Milone, A. P., Bedin, L. R., Cassisi, S., et al. 2013, A&A, 555, A143
Mistry, D., Copperwheat, C. M., Darnley, M. J., & Olier, I. 2022, MNRAS, 517, 3362
Moe, M., & Di Stefano, R. 2017, ApJS, 230, 15
Montalto, M., Piotto, G., Marrese, P. M., et al. 2021, A&A, 653, A98
Mowlavi, N., Holl, B., Lecoeur-Taïbi, I., et al. 2023, A&A, 674, A16
Negueruela, I., Castro, N., & Marco, A. 2023, in Two in a Million – The Interplay Between Binaries and Star Clusters, 39
Netopil, M., Paunzen, E., Heiter, U., & Soubiran, C. 2016, A&A, 585, A150
Netopil, M., Oralhan, İ. A., Çakmak, H., Michel, R., & Karataş, Y. 2022, MNRAS, 509, 421
Nguyen, C. T., Costa, G., Girardi, L., et al. 2022, A&A, 665, A126
Niederhofer, F., Georgy, C., Bastian, N., & Ekström, S. 2015, MNRAS, 453, 2070
Nine, A. C., Mathieu, R. D., Gosnell, N. M., & Leiner, E. M. 2023, ApJ, 944, 145
Ochsenbein, F., Bauer, P., & Marcout, J. 2000, A&AS, 143, 23
Pancino, E., Zocchi, A., Rainer, M., et al. 2024, A&A, 686, A283
Patton, R. A., Pinsonneault, M. H., Cao, L., et al. 2024, MNRAS, 528, 3232
Pawlak, M., Soszyński, I., Udalski, A., et al. 2016, Acta Astron., 66, 421
Perren, G. I., Pera, M. S., Navone, H. D., & Vázquez, R. A. 2023, MNRAS, 526, 4107
Pietrukowicz, P., Soszyński, I., & Udalski, A. 2021, Acta Astron., 71, 205
Pourbaix, D., Tokovinin, A. A., Batten, A. H., et al. 2004, A&A, 424, 727
Price-Whelan, A. M., Hogg, D. W., Rix, H.-W., et al. 2020, ApJ, 895, 2
Qian, S.-B., Shi, X.-D., Zhu, L.-Y., et al. 2019, Res. Astron. Astrophys., 19, 064
Qin, S., Zhong, J., Anders, F., et al. 2026, Res. Astron. Astrophys., 26, 015012
R Core Team. 2017, R: A Language and Environment for Statistical Computing (R Foundation for Statistical Computing, Vienna, Austria)
Raghavan, D., McAlister, H. A., Henry, T. J., et al. 2010, ApJS, 190, 1
Rain, M. J., Ahumada, J. A., & Carraro, G. 2021, A&A, 650, A67
Ramos, A. A., Holanda, N., Drake, N. A., et al. 2024, MNRAS, 527, 6211
Randich, S., Gilmore, G., Magrini, L., et al. 2022, A&A, 666, A121
Rani, S., Pandey, G., Subramaniam, A., & Rao, N. K. 2023, ApJ, 945, 11
Rao, K. K., Vaidya, K., Agarwal, M., et al. 2022, MNRAS, 516, 2444
Recio-Blanco, A., de Laverny, P., Palicio, P. A., et al. 2023, A&A, 674, A29
Reid, M. J., Menten, K. M., Brunthaler, A., et al. 2014, ApJ, 783, 130
Rimoldini, L., Holl, B., Gavras, P., et al. 2023, A&A, 674, A14
Ripepi, V., Clementini, G., Molinaro, R., et al. 2023, A&A, 674, A17
Saketh, P., Panthi, A., & Vaidya, K. 2024, AJ, 168, 97
Sales Silva, J. V., Peña Suárez, V. J., Katime Santrich, O. J., et al. 2014, AJ, 148, 83
Sampedro, L., Dias, W. S., Alfaro, E. J., Monteiro, H., & Molino, A. 2017, MNRAS, 470, 3937
Sandage, A. 1953, Ph.D. Thesis, California Institute of Technology

Sandquist, E. L., Latham, D. W., Shetrone, M. D., & Milone, A. A. E. 2003, AJ, 125, 810
Santos, W., Daflon, S., Silva, J. V. S., et al. 2025, MNRAS, 541, 1449
Sim, G., Lee, S. H., Ann, H. B., & Kim, S. 2019, J. Korean Astron. Soc., 52, 145
Simonian, G. V. A., Pinsonneault, M. H., Terndrup, D. M., & van Saders, J. L. 2020, ApJ, 898, 76
Sindhu, N., Subramaniam, A., Jadhav, V. V., et al. 2019, ApJ, 882, 43
Skumanich, A. 1972, ApJ, 171, 565
Smith, N. 2014, ARA&A, 52, 487
Soberman, G. E., Phinney, E. S., & van den Heuvel, E. P. J. 1997, A&A, 327, 620
Soszyński, I., Pawlak, M., Pietrukowicz, P., et al. 2016, Acta Astron., 66, 405
Soszyński, I., Pietrukowicz, P., Skowron, J., et al. 2021, Acta Astron., 71, 189
Steinmetz, M., Matijevič, G., Enke, H., et al. 2020, AJ, 160, 82
Subramaniam, A., Sindhu, N., Tandon, S. N., et al. 2016, ApJ, 833, L27
Sun, W., Li, C., Deng, L., & de Grijs, R. 2019, ApJ, 883, 182
Sun, M., Levina, S., Gossage, S., et al. 2024, ApJ, 969, 8
Tayar, J., Ceillier, T., García-Hernández, D. A., et al. 2015, ApJ, 807, 82
Taylor, M. B. 2005, ASP Conf. Ser., 347, 29
Tian, H.-J., El-Badry, K., Rix, H.-W., & Gould, A. 2020, ApJS, 246, 4
Traven, G., Feltzing, S., Merle, T., et al. 2020, A&A, 638, A145
Tsantaki, M., Pancino, E., Marrese, P., et al. 2022, A&A, 659, A95
Turchi, A., Pancino, E., Avdeeva, A., et al. 2025, A&A, 700, A195
Wang, C., Langer, N., Schootemeijer, A., et al. 2022, Nat. Astron., 6, 480
Wenger, M., Ochsenbein, F., Egret, D., et al. 2000, A&AS, 143, 9
Zahn, J.-P. 1992, A&A, 265, 115
Zhang, R., Wang, G.-J., Lu, Y., et al. 2024, A&A, 692, A212
Zhao, G., Zhao, Y.-H., Chu, Y.-Q., Jing, Y.-P., & Deng, L.-C. 2012, Res. Astron. Astrophys., 12, 723

Appendix A: More details on sample selection

To integrate the missing clusters in the Hunt & Reffert (2024) catalogue (see Sect. 2.1), we created our own collection of member lists, using the following large literature studies:

– Cantat-Gaudin & Anders (2020) and Cantat-Gaudin et al. (2020), which contain more than 480 000 stars belonging to 2017 clusters; they also homogeneously reanalised clusters previously published by various authors (e.g. Sampedro et al. 2017; Cantat-Gaudin et al. 2018b,a; Castro-Ginard et al. 2018, 2019, and others).
– Sim et al. (2019) did not provide any members lists, so we could not use their work, but we note that of their 207 clusters, 137 are included in Cantat-Gaudin & Anders (2020) and (Cantat-Gaudin et al. 2020).
– Castro-Ginard et al. (2022) provided 25466 members for 628 clusters (615 new), using *Gaia* EDR3.
– Among the clusters by Ferreira et al. (2019, 2020, 2021), we found 26 not included above, with 4539 new member stars.
– He et al. (2021) found 74 new clusters with 3754 members.
– Hao et al. (2022) provided 704 (378 new) clusters with 19425 member stars, using *Gaia* EDR3.

Because some of the above studies were based on *Gaia* DR2 (Gaia Collaboration 2018), we computed a DR2-DR3 cross-match using the software by Marrese et al. (2017, 2019) and used the best matches as our *bona fide* identifications. We identified more than 200 000 member stars in our literature collection that were missing from the Hunt & Reffert (2024) list.

As mentioned in Sect. 2.2, in most cases the CMDs obtained with the Hunt & Reffert (2024) list appear cleaner and better defined, therefore we did not want to blindly merge the two lists. We thus adopted the following approach: we visually inspected the CMDs and vector-point diagrams of all the relevant clusters to identify the ones, like NGC 7789, for which we considered the Hunt & Reffert (2024) selection to be too restrictive in the coordinates or proper motion-parallax planes, compared to the distribution of stars in the region. Only for these clusters, we added back to our masterlist all the stars that were in our literature collection, but were missing from Hunt & Reffert (2024). These extra stars were later retained only if they had rotational information in *Gaia* DR3 (Gaia Collaboration 2023c, see also Sect. 2.3), after checking that the *Gaia* DR3 positions, motions, colors, and magnitudes of the missing stars were still compatible with being cluster members. We also retained all the member stars of the 51 missing clusters in Hunt & Reffert (2024) discussed in Sect. 2.1 above, regardless of their rotational characterization. In this way, we added more than 10 000 stars to our masterlist.

Notably, the list contains some repeated stars, which were assigned as members to different nearby clusters, with different membership probabilities. We decided to keep these duplicates as separate entries in our masterlist.

A.1. Gaia quality selections and additional information

Using the *Gaia* DR3 `source_id` for our stars, we extracted relevant data from the following Gaia Tables:
– `gaia_source`,
– `astrophysical_parameters`,
– `vari_summary`,
– `vari_rotation_modulation`,
– `nss_two_body_orbit`,
– `nss_acceleration_astro`,
– `nss_non_linear_spectro`.

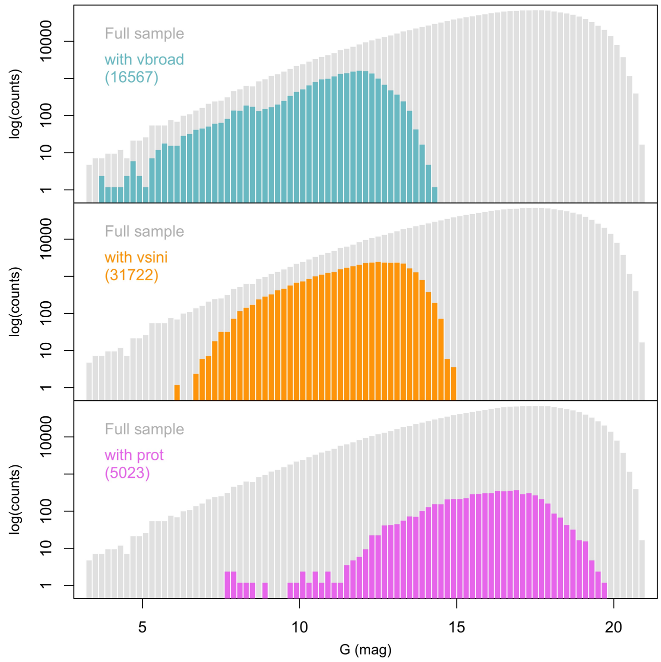

Fig. B.1. Apparent G magnitude distribution of stars with rotation information. In all panels, the full star masterlist is plotted in grey in the background. Stars with a valid `vbroad` parameter are plotted in cyan in the top panel, stars with a valid `vsini` in orange in the middle panel, and stars with a valid `prot` parameter in magenta in the bottom panel (see Secs. B.1, B.2, and B.3 for more details). Sample sizes are listed in parenthesis in each panel.

All stars matching the following criteria, based on information in the above Tables, were rejected from our masterslist:
– sources missing G, BP, or RP magnitudes
– sources with `in_qso_candidates=TRUE`
– sources with `in_galaxy_candidates=TRUE`
– sources with `classprob_dsc_combmod_quasar>0.5`
– sources with `classprob_dsc_combmod_galaxy>0.5`

Apart from these very basic selection criteria, which removed a few hundred stars from the masterlist, we preferred to flag stars rather than to filter them out. This is because we focus on rotating stars, which can have altered colors and magnitudes, whose RV determination could be less precise, and which might be variable or binary and have less precise astrometry as well.

Appendix B: Details on rotational characterization

B.1. Rotational broadening from Gaia RVS spectra

In *Gaia* DR3 the rotational broadening was measured for the first time (Frémat et al. 2023) and is stored in the parameter `vbroad` in the `gaia_source` Table. While there are still some limitations in these measurements, the large sample size and full sky coverage render the catalogue unique and improvements are expected in the next *Gaia* data releases. Briefly, `vbroad` was estimated by cross-correlation of the RVS spectra with broadened synthetic spectra, without correcting for macro-turbulence broadening[8], and filtering rules were applied to the results: *(i)* sources with at least 6 transits were considered; *(ii)* measurements out-

[8] Macroturbulence broadening is expected to be about a few km s^{-1}, depending on the type of star (Doyle et al. 2014; Jonsson et al. 2020).

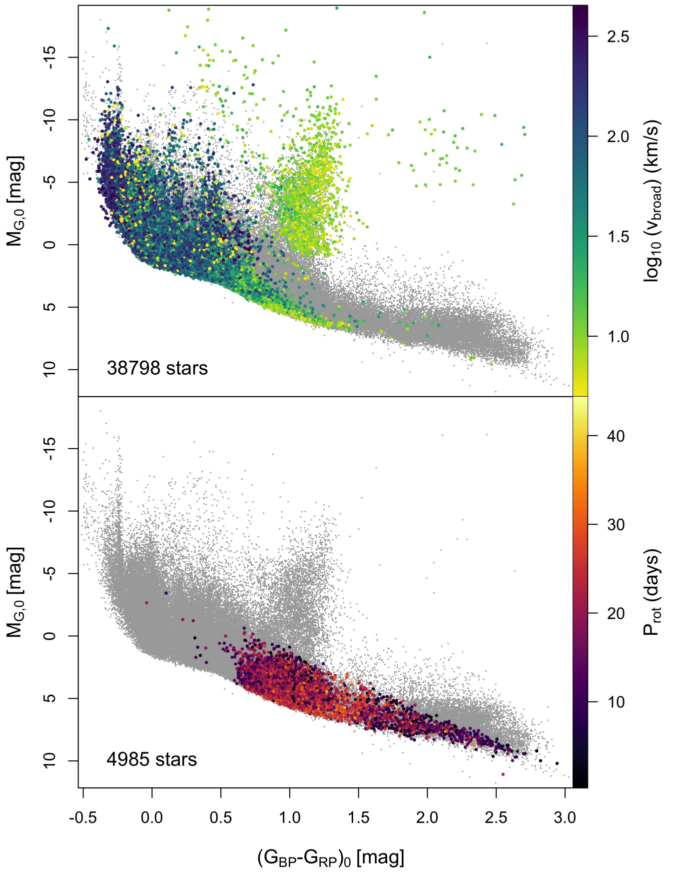

Fig. B.2. Stars with rotation information in *Gaia* DR3, on the absolute and dereddened CMD. Stars with a `vbroad` or `vsini` determination are shown on the top panel, while stars with a `prot` determination in the bottom panel. A selection of well-measured stars from the full sample is plotted in grey in the background, for reference.

side the range $5 < v_{broad} < 500\,\mathrm{km\,s^{-1}}$ were filtered out; *(iii)* only spectra with valid RV measurements were considered, i.e. with $3500 < T_{eff} < 14\,500$ K; and *(iv)* only stars with $G_{RVS} < 12$ mag were analyzed, corresponding to $G \simeq 14.5$ mag (Figure B.1).

A very careful assessment of the reliability of the DR3 `vbroad` measurements was performed with dedicated simulations by Frémat et al. (2023) as a function of T_{eff}, spectral mismatches, G_{RVS}, and the like, as well as extensive comparisons with literature samples, including large spectroscopic surveys. As a result, it appears that `vbroad` tends to be overestimated when it is lower than 8–20 $\mathrm{km\,s^{-1}}$, depending on T_{eff} (see Table 2 by Frémat et al. 2023). At the same time, there is a bias with apparent G_{RVS} magnitude (see Fig. 14 by Frémat et al. 2023), in the sense that stars with $T_{eff} \gtrsim 7500$ K have a more and more underestimated `vbroad` as they become fainter, where the exact magnitude at which this becomes important changes as a function of T_{eff} (see also Fig. 2 and Babusiaux et al. 2023).

B.2. Rotational broadening for stars hotter than 7500 K

The *Gaia* extended stellar parametrisers (ESP) are data analysis modules used in *Gaia* data processing to derive stellar parameters for specific stellar types (see Fouesneau et al. 2023, and

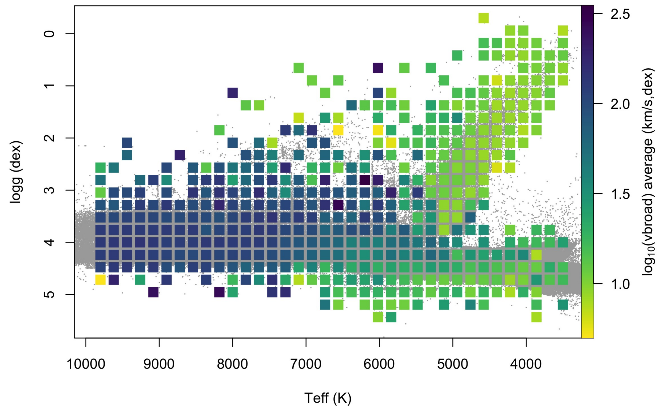

Fig. B.3. The average of `vbroad` or, when missing, `vsini`, in a 2D set of bins in the Kiel diagram. The colorscale is logarithmic to make any subtle variations more visible. In the background, the entire sample is plotted in grey. We left out stars hotter than 10 000 K, we limited the colorscale between 5 and 400 $\mathrm{km\,s^{-1}}$, and we only plotted bins with at least three stars, for clarity.

the *Gaia* online documentation, Sect. 11.3.8[9]). In particular, the ESP dedicated to hot O, B, and A stars (ESP-HS) uses simultaneously the BP/RP and RVS spectra, when available, to derive stellar parameters by comparison with synthetic spectra, specifically suited for these stars. Among them, ESP-HS also derives the projected rotation (`vsini_esphs`, hereafter `vsini`), in case the star has RVS spectra. The results are much more scattered than for `vbroad`, as can be appreciated in Fig. 2 (bottom panels), and as expected in the case of hot stars. However, when we compare the typical uncertainties reported in the *Gaia* DR3 catalogue for `vbroad` and `vsini`, we find the latter to be about a factor of two smaller. We thus multiplied the `vsini` uncertainties by a factor of four before using them in the following analysis. The G magnitude distribution of stars with a `vsini` estimate is shown in Fig. B.1 (middle panel). We observed that `vsini` shows the same trend of `vbroad` in being underestimated for fainter and hotter stars (see also Frémat 2024). Thus, in this work, we mostly focus on `vbroad` rather than `vsini`, unless specifically indicated.

B.3. Rotational periods from Gaia epoch photometry

The *Gaia* multi-epoch photometric data allow for the detailed study of several types of variable stars (Eyer et al. 2023). The determination of rotational periods (`best_rotation_period`, hereafter `prot`) in *Gaia* DR2 and DR3 is based on the flux variability induced by asymmetrically distributed spots on the stellar surface and is only computed for stars of relatively late spectral types in the main sequence ($T_{eff} \lesssim 6\,500$ K, Lanzafame et al. 2018; Distefano et al. 2023). This choice has the additional advantage of minimizing contamination by stellar pulsators. The information is stored in the `vari_rotation_modulation` Table in the *Gaia* archive. An estimate of the chromospheric activity was also obtained as the flux variation amplitude, A_{max} (`max_activity_index_g`). Interestingly, the DR2 sample is not fully included in the DR3 one, thus we downloaded both catalogues. We used our cross-match between DR2 and DR3, described above, to assign a DR3 source ID to sources in the DR2 rotation modulation catalogue. We then merged the two cat-

[9] https://gea.esac.esa.int/archive/documentation/GDR3/Data_analysis/chap_cu8par/sec_cu8par_apsis/ssec_cu8par_apsis_esphs.html

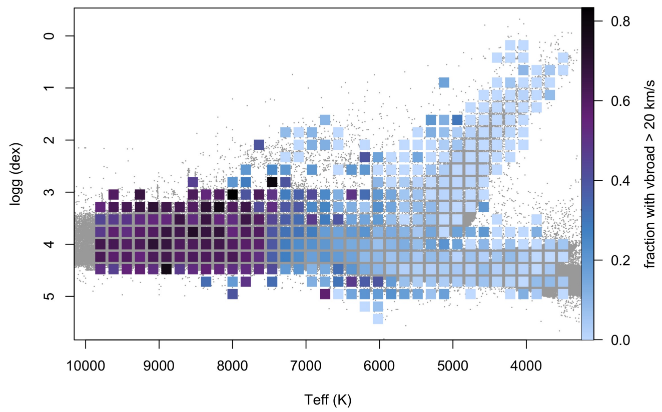

Fig. B.4. Similar to Fig. B.3, but here we plot the fraction of stars with vbroad > 20 km s^{-1}. In the background, the entire sample is plotted in grey. We left out stars hotter than 10 000 K and fainter than G = 14 mag (which could not possibly have a vbroad estimate in *Gaia* DR3). We only plotted bins with at least five stars, for clarity.

alogues. When a source was present in both DR2 and DR3, we selected the DR3 information. The G magnitude distribution of stars with a prot estimate is shown in Fig. B.1 (bottom panel). As can be seen, these stars are generally much fainter than the ones having vbroad or vsini, providing an entirely different window on stellar rotation.

A careful validation of the prot estimates was performed by Lanzafame et al. (2018, for DR2) and Distefano et al. (2023, for DR3), which results in the cleaning of stars with non-optimal time sampling or coverage, in the cleaning of spurious periods, and in a generally favorable comparison with literature samples such as the Zwicky Transient Facility survey (ZTF, Chen et al. 2020), the ASAS-SN survey (Jayasinghe et al. 2021), and several other high-quality literature studies. We note that the particular time sampling of *Gaia* does not allow for a reliable determination of periods larger than a few tens of days. As in the case of vbroad and vsini, the major strength of the prot catalogue lies in its unprecedented size and full-sky coverage, which for example allowed for the definition of a new class of stellar rotators (Lanzafame et al. 2018, 2019, see also Section 3.4).

Appendix C: Sample characterization details

C.1. Stellar radial velocities

We compared the *Gaia* DR3 RVs with the ones in the Survey of Surveys (SoS, Tsantaki et al. 2022), which are obtained by homogenizing, merging, and recalibrating with high-quality samples all the RV measurements by the major spectroscopic surveys. In particular: *Gaia* DR2 (Gaia Collaboration 2018); APOGEE DR16 (Ahumada et al. 2020)[10]; RAVE DR6 (Steinmetz et al. 2020)[11]; GALAH DR2 (Buder et al. 2018)[12]; LAMOST DR5 (Zhao et al. 2012)[13]; and Gaia-ESO DR3 (Gilmore et al. 2012)[14]. No trends are apparent in the DR3 RVs with any of the parameters considered by Tsantaki et al. (2022), while the G magnitude trend previously reported for the DR2 RVs by Katz et al. (2019) and Tsantaki et al. (2022) is more than halved in DR3, reaching a maximum overestimate of about 0.4 km s^{-1} at $G_{RVS} \simeq 14$ mag. We corrected the trend using Equation 5 by Katz et al. (2023). A different trend was observed for stars hotter than 8500 K, which we corrected using Equation 1 by Blomme et al. (2023).

After these corrections, the median difference of the *Gaia* RVs from the SoS ones is –0.06 ± 2.03 km^{-1} for the full sample. As expected, the agreement worsens when considering only stars with vbroad > 50 km s^{-1}, where it becomes –1.56 ± 6.67 km s^{-1}. In any case, the comparison is compatible with the typical precision and accuracy quoted in the respective papers, therefore we adopt the SoS value for ≃6700 faint stars without a *Gaia* RV estimate in DR3. Finally, we added RVs from the latest versions of the surveys, after correcting for the median zero-point with respect to *Gaia* DR3. This way, we could assign a radial velocity estimate to ≃14% of our sample stars. Because our collection of individual RV estimates is larger than the one by Hunt & Reffert (2024), we used it to determine new cluster mean velocities (Sect. C.3). For clusters with at least 10 stars, we also estimated an RV membership, listed in the RV_mem parameter in Table 2.

C.2. Stellar parameters

We used several literature source catalogues, prioritised by their precision, which were estimated with the three-cornered hat method, using the stars in common between pairs of catalogues. We noted that the median differences (i.e. zeropoints) among the quoted catalogues are typically below 100 K in T_{eff}, 0.2 dex in log g, and 0.3 dex in [Fe/H] and they get considerably better (about halved) when considering stars with $4000 < T_{eff} < 7500$ K. We also noted that the spreads in the pairwise comparisons among catalogues are in some cases larger than the sum in quadrature of the quoted uncertainties. This is not a problem for the purpose of the present work, but we stress that the reported uncertainties may be underestimated and should be used with caution. The catalogues we used, in priority order, to assign T_{eff}, log g, and [Fe/H] estimates, are:

– SoS spectroscopic parameters (Turchi et al. 2025);
– spectroscopic surveys parameters from the latest available releases (see Sect. 2.3);
– *Gaia* DR3 spectroscopic parameters from gspspec, after applying the recommended corrections to metallicity and log g (Recio-Blanco et al. 2023), and excluding stars with metallicity lower than –1 dex;
– SoS machine-learning parameters (Turchi et al. 2025);
– machine learning [Fe/H] from Andrae et al. (2023), where we only considered stars with $T_{eff} < 4000$ K and we did not use their T_{eff} and log g parameters;
– Gaia DR3 photometric parameters from gspphot, excluding stars with metallicity lower than –1 dex;
– Gaia DR3 ESPHS parameters for stars hotter than 7 500 K.

This way, we could assign at least a rough estimate of T_{eff} and of log g to ≃49% of our sample stars, and an estimate of [Fe/H] to ≃45% of the sample stars. We note that the typical uncertainties of this collection of parameters are of the order of about 200–500 K in T_{eff}, 0.2–0.5 dex in log g, and 0.2–0.5 dex in [Fe/H], with large variations within the sample across the parameter space. In Fig. B.5 we compare our collected parameters with the latest versions of the main spectroscopic surveys (see Sect. 2.3). As can be seen, there is a good overall agreement, except for stars hotter than about 8000 K or with large vbroad.

For stellar masses and radii, we used the *Gaia* DR3 FLAME results (Final Luminosity Age and Mass Estimator), which were extensively tested (Babusiaux et al. 2023), showing some

[10] https://www.sdss.org/dr16/
[11] https://www.rave-survey.org/
[12] https://www.galah-survey.org/
[13] http://www.lamost.org/public/
[14] https://www.gaia-eso.eu/

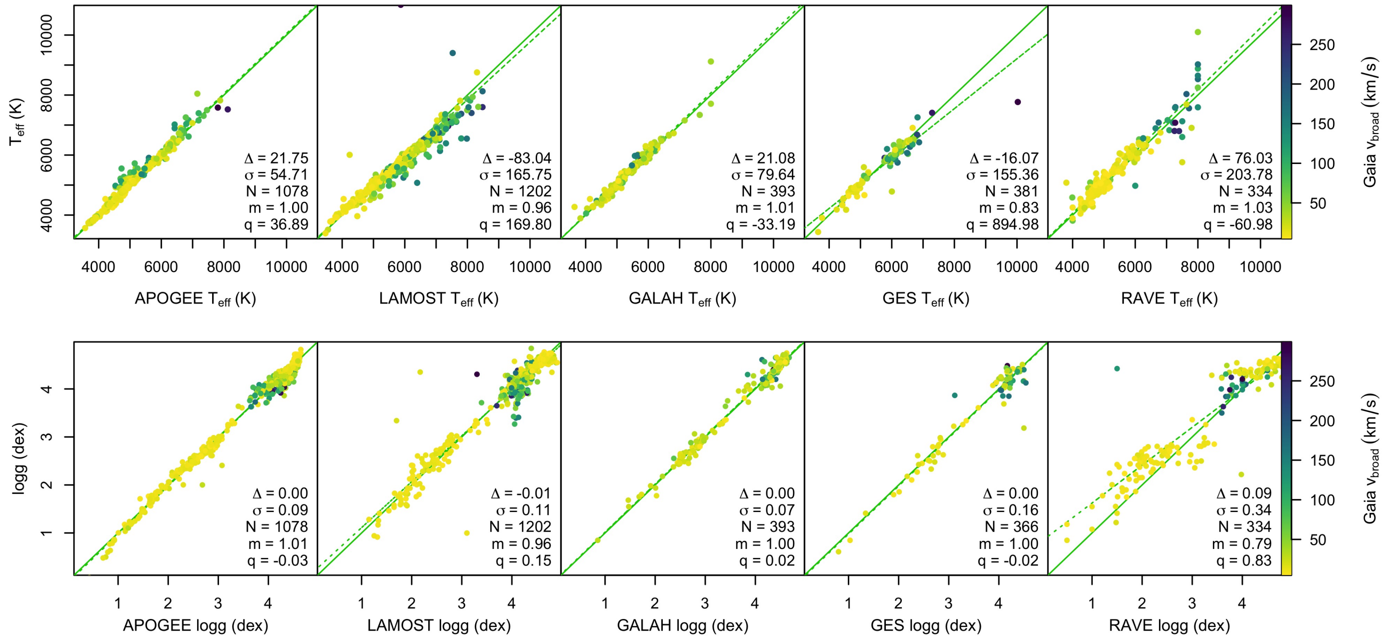

Fig. B.5. Comparison of our selected T_{eff} (top row) and log$g$ (bottom row) parameters with those of the main spectroscopic surveys (see Section B.1 for more details). Each panel reports a different survey as well as the one to one relation (solid green lines) and a linear fit (dashed green lines). The points are colored based on their *Gaia* `vbroad`, where the scale saturates at 300 km s^{-1} to increase plot clarity. The statistics of the comparison and the parameters of linear fits are reported in each panel, labelled as in Figure 2.

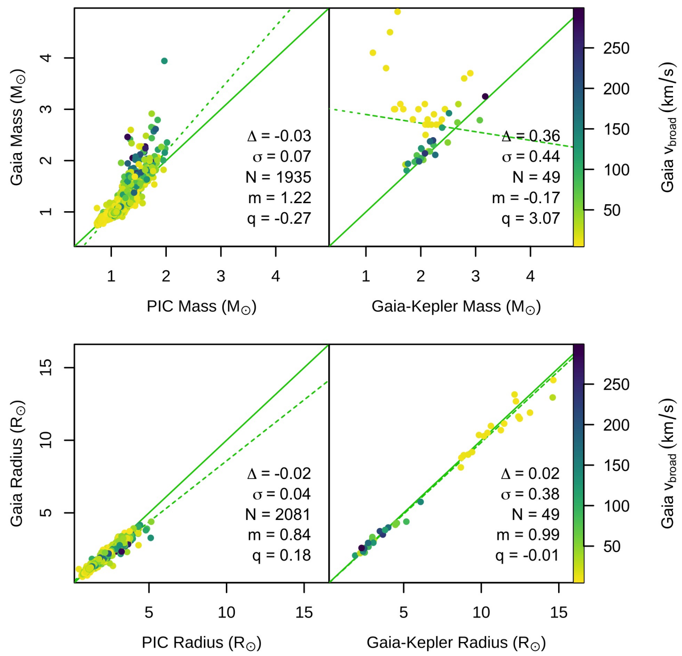

Fig. C.1. Similar to Figure B.5, but for the case of mass (top panels) and radius (bottom panels) estimates. The left panels show the comparison with the PLATO Input Catalogue (PIC, Montalto et al. 2021), and the right ones with the Gaia-Kepler catalogue (Berger et al. 2020). The symbols, annotations, and color-scale are the same as in Figure B.5.

problems only in the high mass range. This is confirmed by our comparison with the PLATO input catalogue (Montalto et al. 2021) and the Gaia-Kepler catalogue (Berger et al. 2020), as illustrated in Fig. C.1. However, for masses lower than about 2.5 $M_{\odot}$ the different datasets agree with each other more than satisfactorily, as well as for radii. We found only mild indications that the *Gaia* FLAME parameters are worse for stars with larger `vbroad` (Fig. C.1, top-right panel).

C.3. Cluster properties

We compared the distance estimates by Hunt & Reffert (2024) against the median of the Bailer-Jones et al. (2021) distances and against the values in our literature collection (Sect. 2.2). We noticed that after about 5 kpc the agreement among these catalogues breaks down and the spread rises to 10-15%, respectively. We attribute this to a parallax bias between *Gaia* DR2 and DR3 of about 0.015 mas (estimated from the two member lists). Indeed the Bailer-Jones et al. (2021) median cluster distances agree better with the Hunt & Reffert (2024) ones than with our literature collection, which is dominated by DR2 estimates. We thus decided to rely on the Hunt & Reffert (2024) estimates and we used the Bailer-Jones et al. (2021) ones for the 51 clusters not included in their catalogue. Cluster masses are taken from Hunt & Reffert (2024).

For mean RVs, we profited from the values collected in our member stars list (Sect. C.2 and Table 2), which come mostly from *Gaia* DR3 (Katz et al. 2023; Blomme et al. 2023) and the SoS (Tsantaki et al. 2022), but also from spectroscopic surveys. This way, we can count on more stars with RV estimated than the ones considered by Hunt & Reffert (2024). We computed cluster median RVs and their spread using the median and the MAD of the members stars in each cluster, after removing all the confirmed binary and variable stars. Our results agree extremely well with the ones by Hunt & Reffert (2024), with a median difference of -0.001 ± 3.249 km s^{-1}, but we could add RV to almost 500 more clusters and more stars per cluster are generally used to obtain each estimate. We included the RV estimates by Dias et al. (2021) for four clusters lacking it. In summary, we obtained a systemic RV estimate for 4980 clusters (≃ 87%), but we note that 2064 clusters have <3 stars with a valid RV estimate.

Cluster metallicities are not present in the Hunt & Reffert (2021, 2023, 2024) catalogue. We thus collected literature results by Dias et al. (2021), Netopil et al. (2016, 2022), Fu et al. (2022), Zhang et al. (2024) for 1571 clusters. We also computed new cluster metallicities from our collection of [Fe/H] estimates, by selecting stars with $-1 <$ [Fe/H] < 0.5 dex, $T_{\rm eff} < 8000$ K, and with metallicity errors below 1 dex. When comparing the literature estimates with each other we obtained values within less than 0.05–0.10 dex from each other. When comparing our newly computed mean cluster metallicities with the literature collection, however, we found offsets of 0.2 dex or more and a very poor correlation. Only once the *Gaia* DR3 individual star estimates were removed from the collection, we could obtain estimates comparable to the ones in the literature, with a difference of Δ[Fe/H] $= 0.03 \pm 0.13$ dex for 980 clusters in common. Merging the two sets, the literature one and our newly computed metallicites, we could assign an average [Fe/H] estimate to 2336 clusters in our sample (about 41%).

Finally, for cluster ages, we noticed that for relatively old clusters ($\gtrsim$500 Myr) with many BSS, the ages by Hunt & Reffert (2023) are severely underestimated, because the isochrone is wrongly adjusted to include the BSS sequence. This is particular evident in their Fig. 6 for the case of Ruprecht 147. For this reason, we preferred the ages by Cavallo et al. (2024) when available. Otherwise, we used Cantat-Gaudin et al. (2020) because of the good agreeement with Cavallo et al. (2024), and in case those were missing, we used Hunt & Reffert (2023).

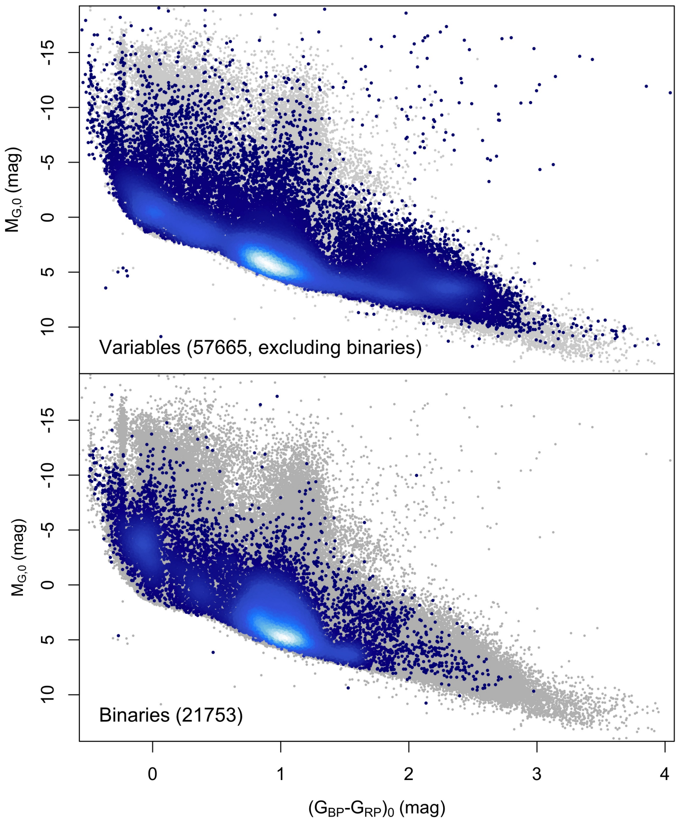

Fig. D.1. Density of variable stars (top panel, excluding binaries) and binary stars (bottom panel) in the absolute and dereddened CMD. Both confirmed and candidate variables and binaries are included. The full sample (Table 2) is plotted in the background as small grey points in both panels.

Appendix D: Variable and binary stars

D.1. Variable stars

Variability information was obtained mainly from the *Gaia* DR3 `vari_summary` and `vari_classifier_result` tables. The enormous amount of work done to classify and characterise the *Gaia* DR3 variables is summarised by Eyer et al. (2023) and more details are provided in a series of papers divided by variable type (Clementini et al. 2023; Gaia Collaboration 2023b; Distefano et al. 2023; Gomel et al. 2023; Lebzelter et al. 2023; Marton et al. 2023; Ripepi et al. 2023). We also profited from the critically compiled catalogue of literature variables by Gavras et al. (2023), which contains an exhaustive selection of publications before 2021. We complemented it with the most updated versions of the ZTF survey (Chen et al. 2020), the ASAS-SN catalogue of variable stars (Jayasinghe et al. 2021), the latest TESS variables classification by Gao et al. (2025). We also checked the updated versions of the main OGLE catalogues[15] (Pawlak et al. 2016; Soszyński et al. 2016; Pietrukowicz et al. 2021; Soszyński et al. 2021; Iwanek et al. 2022, and updates). We finally explored the lists of variable objects found in the *Gaia* science alerts (Hodgkin et al. 2021; Mistry et al. 2022), but we only found stars already included in the above catalogues.

The cross-match of large catalogues with *Gaia* DR3 was performed with the software described by (Marrese et al. 2017, 2019), while the small ones were cross-matched with `TopCat`[16] (Taylor 2005). Some literature catalogues were already cross-matched with *Gaia* DR3 and in those cases we trusted the provided identifications. We did not attempt any homogenization of the literature information, but we reported some of the basic literature information in Table D.1. Based on the available literature information, we set a specific flag in the catalogue of cluster members (Table 2), named `flag_var`, which can take the value `VAR` for confirmed and characterised variable stars, or the value `VAR:` for less secure identifications. To this aim, we employed the available indicators such as figures of merit, classification probability, class identifiers, or conflicting information in the literature. The variable stars sample is presented in Fig. D.1 (upper panel).

D.2. Binary stars

Gaia DR3 presents for the first time the results of the non-single stars pipelines (hereafter NSS, Gaia Collaboration 2023a), which use astrometric (Halbwachs et al. 2023), photometric (Eyer et al. 2023), and spectroscopic time series to detect and to model binary stars (see also Holl et al. 2023; Andrew et al. 2022; Rimoldini et al. 2023; Mowlavi et al. 2023). We use here *Gaia* DR3 data for binaries which were observed for at least one entire orbit and modelled as a two body system (table `nss_two_body_orbit`), as well as those for which the orbit was not closed, but a clear variation in the astrometric solution or in the radial velocities was found (tables `nss_acceleration_astro` and `nss_non_linear_spectro`).

We complemented the *Gaia* binary data with various literature sources, cross-matching them with our sample as described in the previous section. We included binaries from CoRoT (Deleuil et al. 2018) and Kepler (Kirk et al. 2016), as well as

[15] https://ogledb.astrouw.edu.pl/~ogle/OCVS/
[16] https://www.star.bristol.ac.uk/mbt/topcat/

Table D.1. Literature information on variable stars. See Sects. D.1, D.2, and D for more details and references.

Quantity	Units	Description
source_id		*Gaia* DR3 source ID
GAIA_PER	(d)	*Gaia* DR3 period
GAIA_AMP	(mag)	*Gaia* DR3 amplitude
GAIA_NUM		*Gaia* DR3 epochs
GAIA_TYP		*Gaia* DR3 type
GAIA_CLASS		*Gaia* DR3 class
GAIA_SCORE		*Gaia* DR3 score
GAV_PER	(d)	Gavras et al. (2023) period
GAV_TYP		Gavras et al. (2023) superclass
GAV_SRC		Gavras et al. (2023) source
ZTF_ID		ZTF identifier
ZTF_PER	(d)	ZTF period
ZTF_AMP	(mag)	ZTF amplitude
ZTF_NUM		ZTF epochs
ZTF_TYP		ZTF classification
ASA_ID		ASAS-SN identifier
ASA_PER	(d)	ASAS-SN period
ASA_AMP	(mag)	ASAS-SN amplitude
ASA_PROB		ASAS-SN class probability
ASA_TYP		ASAS-SN classification
TES_ID		TESS identifier
TES_PER	(d)	TESS period
TES_AMP	(mag)	TESS amplitude
TES_PROB		TESS class probability
TES_TYP		TESS classification
OGL_ID		OGLE identifier
OGL_PER	(d)	OGLE period
OGL_AMP	(mag)	OGLE amplitude
OGL_TYP		OGLE classification

the latest version of the SB9 catalogue (Pourbaix et al. 2004, March 2021 update). We also included binaries from large spectroscopic surveys and other survey data from a variety of catalogues (e.g. Merle et al. 2017; El-Badry et al. 2018; Birko et al. 2019; Qian et al. 2019; Merle et al. 2020; Mazzola et al. 2020; Price-Whelan et al. 2020; Tian et al. 2020; Traven et al. 2020; Kovalev et al. 2024; Grondin et al. 2024; Jackim et al. 2024).

Similarly to the case of variable stars, we used the available information in the literature catalogues to evaluate the robustness of the binary identification (i.e. number of epochs and various figures of merit). We labelled binaries with `BIN` and candidate or suspected binaries with `BIN:` in a dedicated field (`flag_bin`, see Table 2). All the variable stars of binary nature, such as eclipsing or ellipsoidal variables, and many others, were flagged both as variables and as binaries. As in the case of variable stars, we did not attempt to homogenise the literature classification and parametrization of binaries, but we reported relevant literature information in Table D.2. Our binary star sample is presented in Fig. D.1 (lower panel).

Table D.2. Literature information on binaries or suspected binary stars. See Sects. D.1, D.2, and D for more details and references.

Quantity	Units	Description
source_id		*Gaia* DR3 source ID
NSS_PER	(d)	*Gaia* NSS orbital period
NSS_ECC		*Gaia* NSS orbital eccentricity
NSS_TYP		*Gaia* NSS solution type
SB9_ID		SB9 identifier
SB9_PER	(d)	SB9 orbital period
SB9_ECC		SB9 orbital eccentricity
SB9_TYP		SB9 binary type
SB9_BIB		SB9 reference
KIR_ID		Kirk et al. (2016) identifier
KIR_TYP		Kirk et al. (2016) binary type
DEL_ID		Deleuil et al. (2018) identifier
DEL_PER	(d)	Deleuil et al. (2018) orbital period
DEL_TYP		Deleuil et al. (2018) binary type
ELB_ID		El-Badry et al. (2018) identifier
ELB_TYP		El-Badry et al. (2018) binary type
BIR_ID		Birko et al. (2019) identifier
BIR_TYP		Birko et al. (2019) binary type
QIA_ID		Qian et al. (2019) identifier
QIA_TYP		Qian et al. (2019) binary type
MAZ_ID		Mazzola et al. (2020) identifier
MAZ_TYP		Mazzola et al. (2020) binary type
PRI_ID		Price-Whelan et al. (2020) identifier
PRI_NUM		Price-Whelan et al. (2020) epochs
PRI_PER	(d)	Price-Whelan et al. (2020) period
PRI_ECC		Price-Whelan et al. (2020) eccentricity
PRI_TYP		Price-Whelan et al. (2020) binary type
TIA_ID		Tian et al. (2020) identifier
TIA_PROB		Tian et al. (2020) epochs
TIA_TYP		Tian et al. (2020) binary type
TRA_ID		Traven et al. (2020) identifier
TRA_TYP		Traven et al. (2020) binary type
KOU_ID		Kounkel et al. (2021) identifier
KOU_NUM		Kounkel et al. (2021) epochs
KOU_PER	(d)	Kounkel et al. (2021) period
KOU_ECC		Kounkel et al. (2021) eccentricity
KOU_TYP		Kounkel et al. (2021) binary type
MER_ID		Merle et al. (2017, 2020) identifier
MER_TYP		Merle et al. (2017, 2020) binary type
KOV_ID		Kovalev et al. (2024) identifier
KOV_PER	(d)	Kovalev et al. (2024) period
KOV_ECC		Kovalev et al. (2024) eccentricity
KOV_TYP		Kovalev et al. (2024) binary type
GRO_ID		Grondin et al. (2024) identifier
GRO_TYP		Grondin et al. (2024) binary type
JAC_ID		Jackim et al. (2024) identifier
JAC_TYP		Jackim et al. (2024) binary type

Appendix E: Additional figures and considerations

E.1. Binary fraction

We decided not to use our MS and binMS samples to derive an accurate binary fraction for the sampled clusters. In fact, for clusters with a larger MS spread, we identify binMS with mass ratio q$\gtrsim$0.6, while for those with a much smaller spread, we could also be including q$\gtrsim$0.4 or even lower. A much more accurate assessment, complemented by a differential reddening correction (Pancino et al. 2024), would be required to estimate accurately the fraction of MS binaries with different mass ratios, or to provide a homogeneous sample with q above a fixed value. Moreover, an accurate study of stellar crowding would be required to estimate the number of chance superpositions or blends (Milone et al. 2012), which is beyond the scope of the present paper.

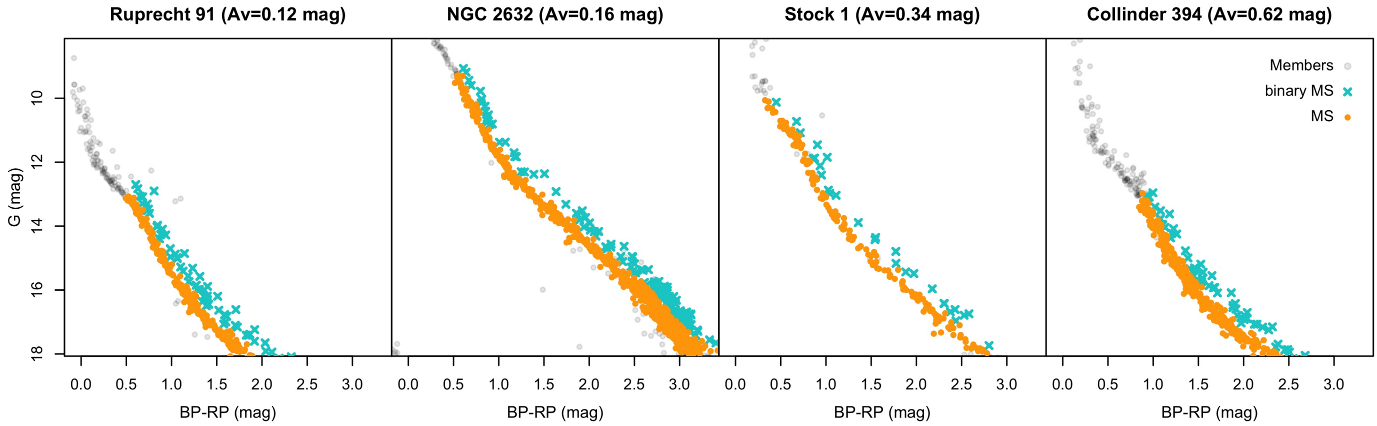

Fig. E.1. Examples of MS and binMS selections. The clusters are plotted in order of increasing interstellar absorption.

Additionally, the method of determining the binary fraction from photometric sequences (first proposed by Kähler 1999) presents two problems. The first is that, below a certain q, binaries land on the MS itself and it is difficult to disentangle them from normal MS stars. For this reason, it is necessary to make assumptions on the q distribution to obtain a binary fraction. Across different field and cluster samples, the q distribution has been found to be flat (Raghavan et al. 2010; Alexander & Albrow 2025), peaking at q≃0.23 (Duquennoy & Mayor 1991), peaking at q≃1 (Fisher et al. 2005), and multi-peak (Moe & Di Stefano 2017). The second problem is that many types of binaries and binary byproducts, including stars out of equilibrium or in particular configurations, also hide within the MS (such as BL). At the same time, many binaries and their byproducts lie outside of the canonical sequences (BSS, subdwarfs, and so on) and are completely excluded if only the MS and binMS are considered.

Thanks to our large compilation of known or suspected binaries from the literature, we are in a position to provide at least some clues on what might be a reasonable q distribution in open clusters. For the MS sample, we find 7% of confirmed binaries, regardless on whether we include or not less certain ones as well (`flag_bin = BIN:`). For the binMS sample, the corresponding figure is 6%. One important factor to consider is that, while it is impossible to correct such a compilation of different methods for detection bias, at the same time the MS and binMS samples should suffer from very similar detection biases. In other words, the discovery fractions reported above should in principle relate to each other in the same way as the actual binary fractions. Our values can thus be used to provide a rough estimate of the ratio between binaries with q≳0.6 and those with q≲0.6, which is about 0.8. This could be a useful indication for future studies of binaries in open clusters. For example, if the q distribution was flat, we would obtain about 0.7.

E.2. Candidate blue lurkers

Lower mass BSS, hidden in the normal MS of M 67 and of other clusters, were discovered by means of their fast rotation (Leiner et al. 2019), which is interpreted as a sign of recent close binary interaction. Similarly to the case of BSS, evidence of close compact companions was found for a few BL so far (Jadhav et al. 2019; Nine et al. 2023; Saketh et al. 2024). According to Leiner et al. (2025), at least one BL was originated in a triple system. Consequently, the operational definition of a BL has shifted in the literature, considering also the UV flux excess, as indicative of a compact companion, as a defining property. The lower masses of BL, compared to BSS, are thought to be caused by a less efficient mass transfer during the interaction (Sun et al. 2024) or by a lower starting mass of the accretor.

In this work, we define BL candidates as stars belonging to the MS or binMS sample of each cluster, with rotation higher than 3 MAD with respect to other stars at a similar magnitude. Our main goal is in fact to decontaminate the MS sample from abnormally fast rotating stars, even if they could be other kinds of interacting binaries. We generally did not consider stars above the point in the MS where the internal structure of the star changes, i.e. the Kraft break (Kraft 1967), especially in clusters with an eMSTO or a split MS. These stars have a large spread in the rotational distribution, which makes it difficult to clearly identify outliers. Therefore, our sample of BL candidates is dominated by low-mass stars, not all of which will be true BL. To this, we add the BL found in the literature (Nine et al. 2023; Jadhav et al. 2019, 2023, 2024, 2026, and Reggiani et al., in preparation). However in the case of NGC 6940 and NGC 752 the literature BL fall onto the eMSTO region and thus we did not consider them here. More in general, we did not flag as BL any star that was already flagged as eMSTO or splitMS. One notable property of our compilation of literature and new BL candidates is that they reach lower ages compared to most literature sources ($6.8 \lesssim \log(\text{age}) \lesssim 9.8$ dex).

The `vbroad` distribution of our BL candidates peaks at about 50 km s^{-1}, with a tail reaching 250 km s^{-1} and above (Fig. 4). About 20% (23 over 113) of the candidate BL are flagged as binaries or suspected binaries, which is about twice the percentage of the MS sample (or the binMS one). They are mostly classified as SB1, with one SB2 and a few astrometric binaries. When the periods are available, they are mostly above 200 days. Eight candidates are classified as RS CVn in *Gaia* DR3 (but not parametrised) and one is an eclipsing binary with a period of 0.9 days in ASAS-SN and Gavras et al. (2023). Many of the candidates were flagged as rotational variables in the literature.

E.3. Additional figures

We place here additional figures with examples of sample selections and specific clusters, relevant to Sect. 3. In particular, Fig. E.1 shows some examples of the separation between the MS and binMS samples, while Fig. E.2 presents a selection of clusters with clean eMSTO and split MS.

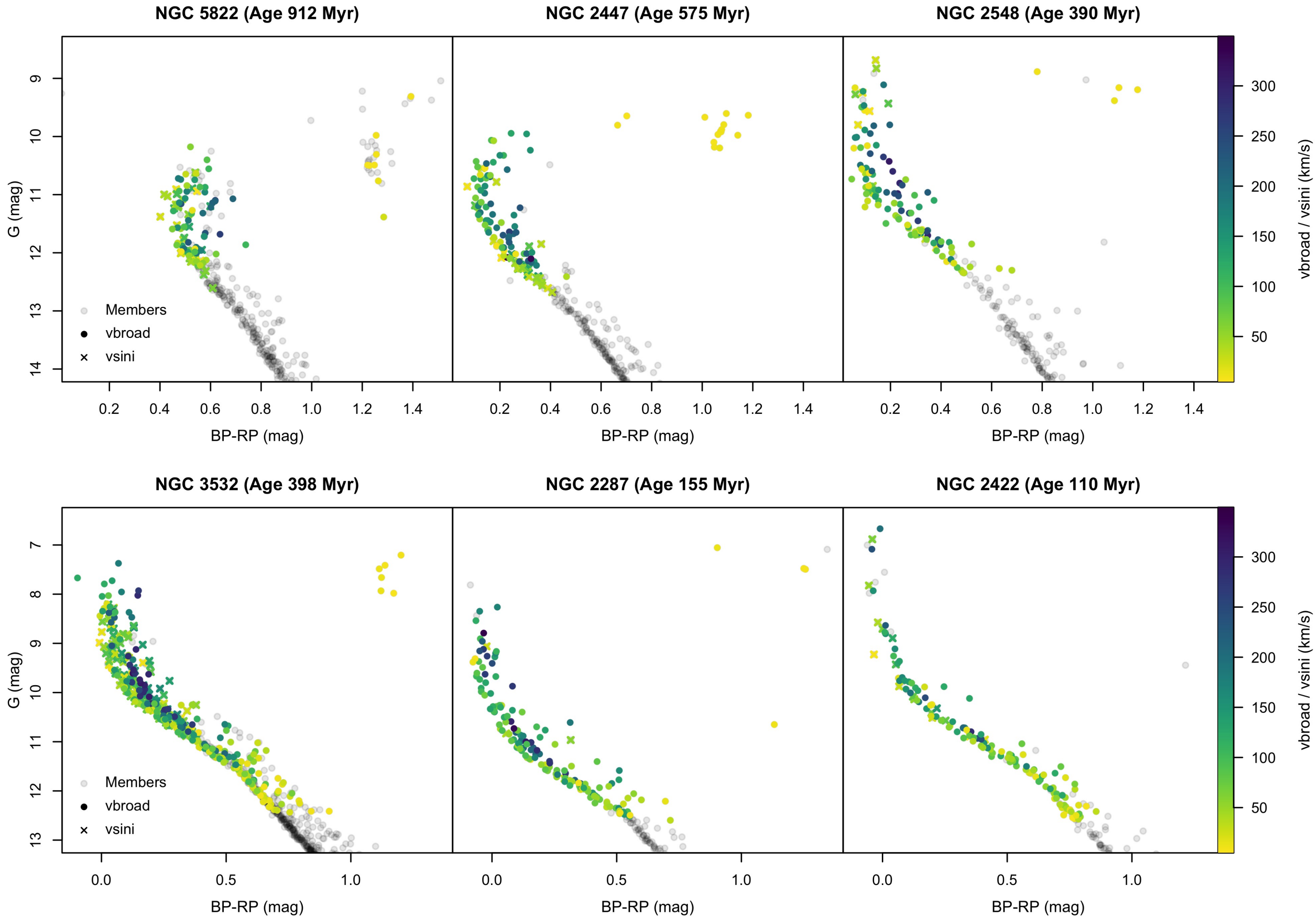

Fig. E.2. Examples of clusters with an eMSTO (top panels) or with a split MS (bottom panels), sorted by decreasing age. The whole cluster sample is plotted in grey in the background, while stars having a `vbroad` estimate are plotted as colored circles and those having a `vsini` estimate are plotted as colored crosses.